$E1$ and $E2$ cross sections of the ^{12}C$(\alpha,\gamma_0)^{16}$O reaction using pulsed α beams

H. Makii,[1,*] Y. Nagai,[1] T. Shima,[1] M. Segawa,[1,†] K. Mishima,[1,‡] H. Ueda,[1,§] M. Igashira,[2] and T. Ohsaki[2,∥]

[1]*Research Center for Nuclear Physics, Osaka University, Ibaraki, Osaka 567-0047, Japan*

[2]*Research Laboratory for Nuclear Reactors, Tokyo Institute of Technology, Meguro, Tokyo 152-8550, Japan*

(Received 3 February 2009; published 3 December 2009)

We measured the γ-ray angular distribution from ^{12}C$(\alpha,\gamma_0)^{16}$O to the ground state of ^{16}O using a pulsed α beam at $E_{\rm eff} = 1.6$ and 1.4 MeV. True events of ^{12}C$(\alpha,\gamma_0)^{16}$O were discriminated from background events with a time-of-flight method because of neutrons from ^{13}C$(\alpha,n)^{16}$O. The obtained γ-ray spectrum with anti-Compton NaI(Tl) spectrometers showed a characteristic line shape from ^{12}C$(\alpha,\gamma_0)^{16}$O: the Doppler broadening and energy loss of α particles in ^{12}C targets. A Rutherford backscattering spectrum of α particles from enriched ^{12}C targets was measured during beam irradiation to obtain the target thickness and incident α-beam intensities. The astrophysical S factors for $E1$ and $E2$, $S_{E1}(\gamma_0 : E_{\rm eff})$ and $S_{E2}(\gamma_0 : E_{\rm eff})$, derived from the present cross sections are in excellent agreement with the values derived by R-matrix calculation of the β-delayed α spectrum of ^{16}N, and by using the asymptotic normalization constant in the R-matrix fit.

DOI: 10.1103/PhysRevC.80.065802 PACS number(s): 25.55.−e, 23.20.En, 27.20.+n

I. INTRODUCTION

The ^{12}C$(\alpha,\gamma)^{16}$O reaction plays an important role in determining the mass fraction of ^{12}C and ^{16}O after stellar helium burning, the abundance distribution of elements between carbon and iron, and the iron-core mass before a supernova explosion [1,2]. To reliably estimate the quantities mentioned using stellar models, the reaction cross section, $\sigma_{\rm tot}$(300 keV), must be determined accurately within an uncertainty of 20% at the Gamow energy (300 keV). However, a direct measurement of $\sigma_{\rm tot}$(300 keV) is not possible using the current experimental techniques, since the cross section, $\sigma_{\rm tot}$(300 keV), is too low (on the order of 10^{-17} b), to be measured in terrestrial laboratories [3]. Hence, $\sigma_{\rm tot}$(300 keV) is derived by extrapolating a measured cross section, $\sigma_{\rm tot}(E_{\rm c.m.})$, at a center of mass (c.m.) energy of $E_{\rm c.m.} \geqslant 1.0$ MeV into the Gamow window based on theoretical calculations, such as K- [4] and R-matrix theories [5–7] and/or microscopic models.

The cross section $\sigma_{\rm tot}$(300 keV) is dominated by the partial cross section, $\sigma(\gamma_0 : 300$ keV), corresponding to the γ-ray transition from ^{12}C$(\alpha,\gamma)^{16}$O to the ground state of ^{16}O [hereafter ^{12}C$(\alpha,\gamma_0)^{16}$O] [8]. The γ-ray transition strength is constituted by two components, the electric dipole ($E1$) and the electric quadrupole ($E2$) multipolarities, because there are several 1^- and 2^+ states in ^{16}O relevant to the ^{12}C$(\alpha,\gamma_0)^{16}$O reaction at stellar energy, which are the high-energy 1^- resonance state (at $E_{\rm c.m.} = 2.418$ MeV), the subthreshold 1^- (at $E_{\rm c.m.} = -0.045$ MeV) and 2^+ (at $E_{\rm c.m.} = -0.245$ MeV) states, and high-energy 2^+ resonances (at $E_{\rm c.m.} = 2.68$ and 4.36 MeV), respectively [9], as shown in Fig. 1. The tails of the 1^- states mentioned contribute to the $E1$ cross section to the ground state, $\sigma_{E1}(\gamma_0 : 300$ keV). Any interference with the direct $E2$-capture process into the ground state of ^{16}O, capture into the tail of the subthreshold 2^+ state, and captures into the tails of the high-energy 2^+ resonances contributes to the $E2$ cross section, $\sigma_{E2}(\gamma_0 : 300$ keV).

Because of different properties of these 1^- and 2^+ states, such as their excitation energies and widths, the energy dependence of $\sigma_{E1}(\gamma_0 : E_{\rm c.m.})$ differs from that of $\sigma_{E2}(\gamma_0 : E_{\rm c.m.})$. Hence, extensive studies were carried out to determine separately $\sigma_{E1}(\gamma_0 : E_{\rm c.m.})$ and $\sigma_{E2}(\gamma_0 : E_{\rm c.m.})$, as described here. Note that both experimental and theoretical studies of radiative α-particle capture into excited states of ^{16}O, such as the 6.92-MeV ($J^\pi = 2^+$) and 6.05-MeV ($J^\pi = 0^+$) states, have also been conducted to obtain their contribution to $\sigma_{\rm tot}$(300 keV) [10]. The strongest contribution to an astrophysical total S factor at the Gamow energy, $S_{\rm tot}$(300 keV), from cascade transitions was claimed to be due to the capture into the 6.05-MeV state [11], which is about 15% of the total $S_{\rm tot}$(300 keV).

II. PREVIOUS WORK

The first successful $\sigma(\gamma_0 : E_{\rm c.m.})$ measurement was carried out at $1.41 \leqslant E_{\rm c.m.} \leqslant 2.94$ MeV by Dyer and Barnes [3]. They found the principal difficulty of the measurement to arise from the combination of low γ-ray yield resulting from a very small $\sigma(\gamma_0 : E_{\rm c.m.})$ and high background events due to neutrons from ^{13}C$(\alpha,n)^{16}$O. Note that the cross section of ^{13}C$(\alpha,n)^{16}$O with a Q value of +2.21 MeV is so large, about 10^7 times larger than that of ^{12}C$(\alpha,\gamma_0)^{16}$O [12], that any contamination of ^{13}C in the target and/or a target backing is undesirable. In fact, Dyer and Barnes used an enriched ^{12}C target to reduce the amount of ^{13}C, a pulsed α beam to separate neutron background events from true γ-ray events resulting from ^{12}C$(\alpha,\gamma_0)^{16}$O with a time-of-flight (TOF) method, and a

*Present address: Advanced Science Research Center, Japan Atomic Energy Agency (JAEA), Tokai, Ibaraki 319-1195, Japan.

†Present address: Quantum Beam Science Directorate, Japan Atomic Energy Agency (JAEA), Tokai, Ibaraki 319-1195, Japan.

‡Present address: Institute of Materials Structure Science, High Energy Accelerator Research Organization (KEK), Tsukuba, Ibaraki 305-0801, Japan.

§Present address: Nippon Advanced Technology Corporation, Tokai, Ibaraki 319-1112, Japan.

∥Present address: Intellectual Property Bank Corporation, Minato, Tokyo 105-0001, Japan.

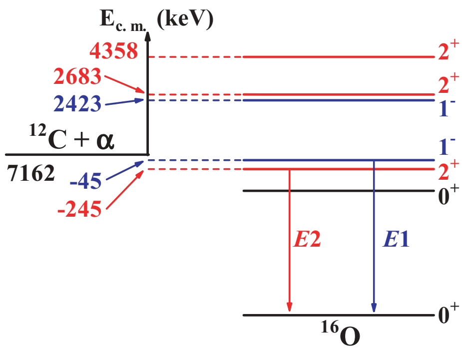

FIG. 1. (Color online) Partial level scheme of ^{16}O, relevant to the $^{12}C(\alpha,\gamma_0)^{16}O$ reaction at low energy. The γ-ray transition strength comprises the $E1$ and the $E2$ multipolarities, since there are several 1^- and 2^+ states in ^{16}O, as shown here.

large-volume NaI(Tl) detector to detect the γ ray. They also pointed out an important contribution of $\sigma_{E2}(\gamma_0 : E_{c.m.})$ to $\sigma_{tot}(E_{c.m.})$ at low energy.

Since then, reaction studies have been carried out to determine $\sigma_{E1}(\gamma_0 : E_{c.m.})$; $\sigma_{E2}(\gamma_0 : E_{c.m.})$; the partial cross section, $\sigma(\gamma_0 : E_{c.m.})$; the total cross section including cascade γ-rays, $\sigma_{tot}(E_{c.m.})$; and the cross section for the cascade γ-ray transitions over the past 30 years [10,11,13–20]. The previous value of $S_{E1}(\gamma_0 : E_{c.m.})$ and the ratio of $\sigma_{E2}(\gamma_0 : E_{c.m.})$ to $\sigma_{E1}(\gamma_0 : E_{c.m.})$ are shown in Figs. 2(a) and 2(b), respectively. In these studies, the $^{12}C(\alpha,\gamma)^{16}O$ reaction [10,15,17,20] and/or the inverse $^4He(^{12}C,\gamma)^{16}O$ reaction [11,13,14,16,18,19] were used. The former studies were carried out using an intense continuous α beam and an enriched ^{12}C target implanted into gold to obtain a high γ-ray yield from the reaction and to further deplete the amount of ^{13}C, respectively. Multiple Ge detectors were used to detect true γ-ray events with high efficiency and good energy resolution. Some of the latter studies, being expected to have little contamination of ^{13}C, were made using a recoil separator to clearly pick up true γ-ray events [11,14,19].

Here, it is worth mentioning that after the experiments by Dyer and Barnes [3] and by Kettner *et al.* [13], an averaged value $\sigma(\gamma_0 : E_{c.m.} = 2.36$ MeV) of 47 $\pm$ 3 nb was used to derive a cross section, $\sigma(\gamma_0 : E_{c.m.})$, at low energy of $E_{c.m.}$, except for the latest measurement [20]. Note that the averaged value was obtained by using the $\sigma_{E1}(\gamma_0 : E_{c.m.} = 2.32$ MeV) of 39.53 $\pm$ 1.31 nb [3], the $\sigma(\gamma_0 : E_{c.m.} = 2.36$ MeV) of 53 $\pm$ 4 nb [13], and the $\sigma(\gamma_0 : E_{c.m.} = 2.36$ MeV) of 46 $\pm$ 4 nb [10]. Although it was natural to use the averaged value, which was obtained by independent measurements, $\sigma_{E1}(\gamma_0 : E_{c.m.} =$ 2.32 MeV) [3] differs from $\sigma(\gamma_0 : E_{c.m.} = 2.36$ MeV) [13] by about 25% outside their reported experimental uncertainties. In fact, because a systematic uncertainty of about 10% was reported in the data by Dyer and Barnes, we took a quadratic sum of statistic and systematic errors to evaluate the total uncertainty. The obtained $\sigma_{E1}(\gamma_0 : E_{c.m.} = 2.32$ MeV) of 39.5 $\pm$ 4.2 nb still does not agree with that from Ref. [13], which suggests that there remains an additional unknown systematic uncertainty in the previous $\sigma_{E1}(\gamma_0 : E_{c.m.})$ data. However, the latest result of $\sigma_{E1}(\gamma_0 : E_{c.m.} = 1.34$ MeV), 0.16 $\pm$ 0.06 nb

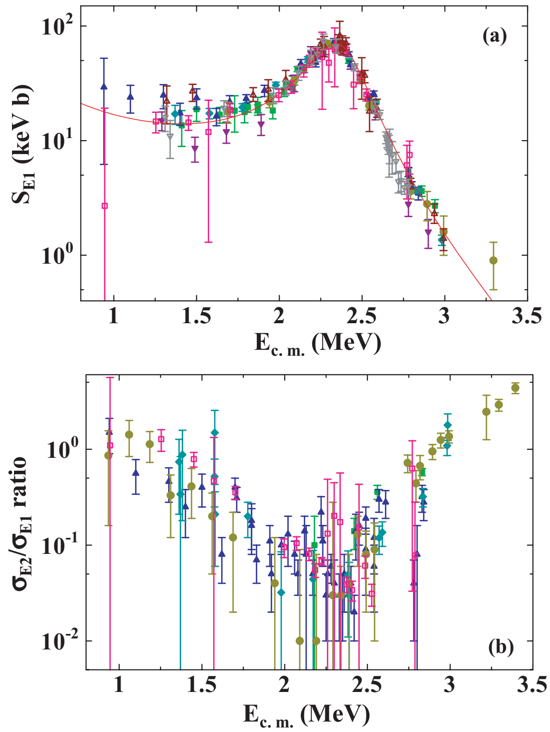

FIG. 2. (Color online) Previous data of an astrophysical S factor for $E1$, $S_{E1}(\gamma_0 : E_{c.m.})$ (a), and of the ratio of $E2$ cross section to the $E1$ cross section (b) (filled rectangle [3], filled triangle [10], filled reverse triangle [14], filled diamond [15], filled circle [16], open rectangle [17], open triangle [18], open reverse triangle [20], and solid line [21]).

[20], was compared to the value of 0.29 $\pm$ 0.10 nb at $E_{c.m.} = 1.41$ MeV by Dyer and Barnes.

A unique method was developed to accurately derive $\sigma_{E1}(\gamma_0 : 300$ keV), in which R- or K-matrix fits were made to the measured spectrum of the α particle from the β decay of ^{16}N, the measured $^{12}C(\alpha,\gamma_0)^{16}O$ cross section, and the measured α + ^{12}C elastic-scattering phase shifts [8,21,22]. Since the α spectrum is sensitive to the reduced α width of the subthreshold 1^- state, the thus-derived $\sigma_{E1}(\gamma_0 :$ 300 keV) is considered to be determined within an uncertainty of 30%. Note that the $S_{E1}(\gamma_0 : 300$ keV) factor extracted from the β-delayed α-decay spectrum from ^{16}N using the R-matrix formalism is known to be quite sensitive to the input parameters, such as $\sigma_{E1}(\gamma_0 : E_{c.m.})$, phase-shift parameters, and the β-branching ratio of the subthreshold 1^- state. Hence, the origin of the mentioned discrepancy of $\sigma_{E1}(\gamma_0 : E_{c.m.})$ between different data sets should be clarified to accurately determine $\sigma_{E1}(\gamma_0 : E_{c.m.})$.

The cross section for $E2, \sigma_{E2}(\gamma_0 : E_{c.m.})$, was derived by using a measured ratio of $\sigma_{E2}(\gamma_0 : E_{c.m.})$ to $\sigma_{E1}(\gamma_0 : E_{c.m.})$, $R = \sigma_{E2}(\gamma_0 : E_{c.m.})/\sigma_{E1}(\gamma_0 : E_{c.m.})$. Here, R was obtained by either measuring the γ-ray angular distribution of $^{12}C(\alpha,\gamma_0)^{16}O$ or by measuring the γ ray from $^{12}C(\alpha,\gamma_0)^{16}O$ at $\theta_\gamma = 90^\circ$ both in far and close geometries of a γ-ray detector. The measured data also provided $\sigma_{E1}(\gamma_0 : E_{c.m.})$ by employing the normalization method mentioned previously. The $E1$ contribution in a close-geometry measurement was corrected for by using the result in a far-geometry measurement [14], which contained predominantly the $E1$ component. The thus-determined ratio, R, has a large uncertainty at $1 < E_{\rm c.m.} < 2.5$ MeV, as shown in Fig. 2(b), and therefore the uncertainty of $\sigma_{E2}(\gamma_0 : E_{\rm c.m.})$ is quite large. It should be noted that like the method in the case mentioned concerning the reduced α width of the subthreshold 1^- state, a unique method was developed to derive $\sigma_{E2}(\gamma_0 : 300$ keV). The reduced α widths of the subthreshold 2^+ and 1^- states were obtained by measuring the total cross sections for the ^{12}C(^{6}Li,d)^{16}O and ^{12}C(^{7}Li,t)^{16}O reactions [23,24]. The obtained data were analyzed together with the measured capture and the phase-shift data to derive the $S_{E2}(\gamma_0 : 300$ keV) factor as well as the $S_{E1}(\gamma_0 : 300$ keV) factor. Quite recently, Dufour and Descouvemont derived an accurate $S_{E2}(\gamma_0 : 300$ keV) value using the α width of the 2^+ state mentioned by constraining the R-matrix analysis on the basis of the generator-coordinate-method asymptotic normalization constant of the 2^+ state and using previous data of $\sigma_{E2}(\gamma_0 : E_{\rm c.m.})$ [7]. Here, it should be mentioned that although the calculated $S_{E2}(\gamma_0 : 300$ keV) factor does not depend on the interference signs of the 2^+ states relevant to ^{12}C(α,γ_0)^{16}O, an accurate $\sigma_{E2}(\gamma_0 : E_{\rm c.m.})$ is required to determine the signs properly and thereby to reliably determine $S_{E2}(\gamma_0 : 300$ keV) based on the model mentioned. Despite experimental progress achieved so far, problems remain concerning the absolute values of $\sigma_{E1}(\gamma_0 : E_{\rm c.m.})$ and $\sigma_{E2}(\gamma_0 : E_{\rm c.m.})$, as mentioned previously, which prompted us to make a new, independent measurement to accurately determine the cross sections. Here, we note that the lowest energy, with the energy that many groups measured [$\sigma_{E2}(\gamma_0 : E_{\rm c.m.})$] by employing independent methods, was around $E_{\rm c.m.} \sim 1.4$ MeV. Hence, in the present study, we aimed to accurately measure $\sigma_{E1}(\gamma_0 : E_{\rm c.m.})$ and $\sigma_{E2}(\gamma_0 : E_{\rm c.m.})$ at $E_{\rm c.m.} = 1.6$ and 1.4 MeV by constructing a new measurement system [25], which would enable us to critically compare the obtained results with previous data and theoretical predictions.

III. EXPERIMENTAL METHOD AND PROCEDURE

A measurement of the γ-ray angular distribution from ^{12}C(α,γ_0)^{16}O was carried out using a newly constructed measurement system at the Research Laboratory for Nuclear Reactors at the Tokyo Institute of Technology.

A. New measurement system

In designing a new system, we first reconsidered the characteristic features of the γ ray from ^{12}C(α,γ_0)^{16}O, which could allow us to unambiguously discriminate the γ-ray events from background events. The γ-ray peak energy should be equal to $7.162 + (12/16) \times E_\alpha$ (in units of MeV) at the laboratory energy E_α after correcting for the Doppler shift of the γ ray, which depends on the detected angle of the γ ray with respect to the α-beam direction, and the energy loss of incident α particles in enriched carbon targets. To unambiguously determine the peak energy of the γ ray, it is necessary to obtain a sufficient γ-ray yield from ^{12}C(α,γ_0)^{16}O with a good signal-to-noise ratio by suppressing background events due to neutrons from ^{13}C(α,n)^{16}O. We could not prepare enriched ^{12}C targets that were entirely free from contamination of ^{13}C. Hence, we used a pulsed α beam to discriminate true γ-ray events attributable to ^{12}C(α,γ_0)^{16}O from neutron-induced background events attributable to neutrons from ^{13}C(α,n)^{16}O with a TOF method, and we used a large-volume anti-Compton NaI(Tl) spectrometer to detect the γ-ray events with high efficiency.

A pulsed α beam was provided from the 3.2-MV Pelletron accelerator at the Tokyo Institute of Technology. Typical averaged α-beam intensity was about 8 μA at a repetition rate of 4 MHz. The pulse width of the α beam was measured to be 1.9 ns full width at half maximum (FWHM) using a plastic scintillation counter [25]. The absolute value of the acceleration voltage was calibrated using the ^{27}Al(p,γ)^{28}Si reaction at three resonances of $E_p = 0.992$, 1.317, and 2.046 MeV and at a threshold energy of 1.879 MeV for the ^{7}Li(p,n)^{7}Be reaction within uncertainties of 1 keV.

We took the Rutherford backscattering (RBS) spectrum of α particles by an enriched ^{12}C target with a gold backing during α-beam irradiation to measure the target thickness. Consequently, we could accurately determine both the effective reaction energy associated with detected γ-ray events and the incident α-beam intensity. These features of the new measurement system could allow us to accurately determine both $\sigma_{E1}(\gamma_0 : E_{\rm c.m.})$ and $\sigma_{E2}(\gamma_0 : E_{\rm c.m.})$ at $E_{\rm c.m.} \approx$ 1.4–1.6 MeV. A detailed description of the new system was published elsewhere [25].

B. Enriched ^{12}C targets and target chamber

Enriched carbon targets (99.95% enrichment in ^{12}C) with a gold backing were made by the thermal cracking of methane gas [26]. These targets with thicknesses of ~250 to 400 μg/cm^2 were strong against intense α-beam irradiation. Note that we introduced unfocused α beams on the ^{12}C targets, in which a tantalum slit with a size of 21×21mm^2 was used to remove a halo beam. We made the target chamber with aluminum, not iron, because the neutron-capture cross section of aluminum is nearly an order of magnitude smaller than that of iron [27]. Note that neutrons of up to about 4 MeV, which were produced by ^{13}C(α,n)^{16}O at $E_\alpha \sim 2$ MeV, could be captured by any materials in the measurement room and would produce a γ-ray background with an energy as great as 8 to 10 MeV, comparable to the characteristic γ-ray energy of $7.162 + (12/16) \times E_\alpha$ MeV from ^{12}C(α,γ_0)^{16}O. To attenuate background γ-ray events resulting from the ($n,n'\gamma$) and (n,γ) reactions by materials around the target chamber, several lead blocks were carefully placed around the chamber so as not to attenuate the characteristic γ-ray events from ^{12}C(α,γ_0)^{16}O.

C. The γ-ray spectrometer

Three large-volume anti-Compton NaI(Tl) spectrometers of the same size were used to simultaneously measure the γ-ray angular distribution of ^{12}C(α,γ_0)^{16}O at $\theta_\gamma = 40^\circ$, 90°, and 130° with respect to the α-beam direction. Each spectrometer consisted of a central NaI(Tl) detector with a diameter of

228.6 mm and a length of 203.2 mm surrounded by an annular NaI(Tl) detector 50.8 mm thick and 368.3 mm long [28]. The energy resolution of the NaI(Tl) detector was about 250 keV (FWHM) at $E_\gamma = 8.5$ MeV. It was compared to an energy spread of about 400 keV, resulting from the α-beam energy loss in a target with a thickness of about 300 μg/cm^2 and the Doppler shift of the γ rays. Boron-doped polyethylene blocks (15% of B_2O_3 in weight) were placed in front of the central NaI(Tl) detector to attenuate the neutron intensity from ^{13}C$(\alpha,n)^{16}$O. The distance between a ^{12}C target and the front face of the central NaI(Tl) detector was 33 cm, which was required to discriminate γ-ray events due to ^{12}C$(\alpha,\gamma_0)^{16}$O from background events induced by ~4 MeV neutrons with a TOF method.

The circuit for the NaI(Tl) spectrometers is briefly described here. A dynode signal from the central NaI(Tl) detector was used as a start signal for a time-to-digital converter (TDC), and the stop signal was obtained from the output of a capacitive pick off to pick up α beam signals. Anode signals from the both central and annular NaI(Tl) detectors were used as energy signals for an analog-to-digital converter (ADC). The threshold energy level of the annular detector was set quite low, at about 45 keV, to effectively suppress the contribution of Compton background γ rays escaping from the central NaI(Tl) detector. The discrimination level of the constant fraction discriminator (CFD) for γ rays detected by the central NaI(Tl) detector was set at about 1 MeV to reduce the total count rate of the data-intake system. Data from Modular Instrumentation and Digital Interface System for Computer Automated Measurement and Control (CAMAC) modules (ADC and TDC) were acquired by a personal computer and recorded on a hard disk in the list mode. The dead time of the system was less than a few percent during the measurement, because the typical count rate was as slow as 1000 counts/s.

Energy calibration of the NaI(Tl) detector was made using the 0.898-, 1.173-, 1.333-, and 1.836-MeV γ rays from the γ-ray standard sources ^{60}Co and ^{88}Y and 1.779-, 2.839-, 5.110-, 8.940-, and 10.763-MeV ones from ^{27}Al$(p,\gamma)^{28}$Si measured at $E_p = 992$ and 2046 keV. The pulse height of the detectors was checked frequently, typically every 4–8 h, with γ rays from neutron-induced reactions, such as 1.720-, 2.614-, and 6.836-MeV γ rays from the ^{27}Al$(n,n'\gamma)^{27}$Al, ^{208}Pb$(n,n'\gamma)^{208}$Pb, and ^{127}I$(n,\gamma)^{128}$I reactions, respectively. Any shift of the γ-ray peak was corrected for during an offline analysis, because data were recorded in the list mode. Consequently, we could determine the energy of an observed γ ray within an uncertainty of 25 keV. Note that one had to accurately determine the energy of observed γ rays resulting from α-beam bombardment on ^{12}C targets to unambiguously identify the γ-ray events from ^{12}C$(\alpha,\gamma_0)^{16}$O.

D. RBS spectrum

We took the RBS spectrum of α particles from ^{12}C targets during α-beam irradiation by means of a Si detector with an active area of 25 mm^2 and a thickness of 100 μm. The Si detector was placed 55 cm behind a ^{12}C target at $\theta_\alpha = 177^\circ$ with respect to the α-beam direction. The detector was covered with a slit with a diameter of 0.2 mm to measure the RBS spectrum free from a pulse pileup and with a slight dead time. The slit size was determined within an uncertainty of 3% by measuring the slit area from a microscope image and also by comparing the α-ray yield from the ^{241}Am α-ray source with that measured using a calibrated slit with an uncertainty of 3% on an Olympus scanning tunneling microscope. The energy calibration of the detector was made using the ^{27}Al$(\alpha,\alpha)^{27}$Al and ^{197}Au$(\alpha,\alpha)^{197}$Au reactions and the ^{241}Am α-source. The energy resolution of the detector, typically 15 keV, was monitored during the measurement of ^{12}C$(\alpha,\gamma_0)^{16}$O using ^{27}Al and ^{197}Au. When the resolution became worse as a result of radiation damage, we replaced it with a new one.

E. Measurement of γ-ray angular distribution

Three angles of $\theta_\gamma = 40^\circ$, 90°, and 130° of three NaI(Tl) spectrometers were chosen by considering characteristic features of the γ-ray angular distribution of ^{12}C$(\alpha,\gamma_0)^{16}$O, given here [3]:

$$\begin{aligned}\frac{d\sigma(E_{\mathrm{c.m.}},\theta)}{d\Omega} &= \frac{\sigma_{E1}(\gamma_0:E_{\mathrm{c.m.}})}{4\pi}\times\Bigg\{1-Q_2P_2(\cos\theta)+\frac{\sigma_{E2}(\gamma_0:E_{\mathrm{c.m.}})}{\sigma_{E1}(\gamma_0:E_{\mathrm{c.m.}})}\\ &\quad\times\left[1+\frac{5}{7}Q_2P_2(\cos\theta)-\frac{12}{7}Q_4P_4(\cos\theta)\right]\\ &\quad+\frac{6\sqrt{5}}{5}\left[\frac{\sigma_{E2}(\gamma_0:E_{\mathrm{c.m.}})}{\sigma_{E1}(\gamma_0:E_{\mathrm{c.m.}})}\right]^{1/2}\cos\Phi(E_{\mathrm{c.m.}})\\ &\quad\times\left[Q_1P_1(\cos\theta)-Q_3P_3(\cos\theta)\right]\Bigg\}. \qquad (1)\end{aligned}$$

Here, $\sigma_{E1}(\gamma_0:E_{\mathrm{c.m.}})$ and $\sigma_{E2}(\gamma_0:E_{\mathrm{c.m.}})$ are the $E1$ and $E2$ cross sections, respectively. The parameter $\Phi(E_{\mathrm{c.m.}})$ is the relative phase between the $E1$ and $E2$ amplitudes. $P_\ell(\ell = 1\sim 4)$ are Legendre polynomials, and Q_m ($m = 1$–4) are attenuation factors of a NaI(Tl) detector, which represent the smearing of the angular distribution resulting from the finite size of the NaI(Tl) detector, respectively. In the present study, we used the phase shift Φ (fixed), which could be determined accurately, as suggested by Barker [29], via the ^{12}C$(\alpha,\alpha)^{12}$C experiments at $1.5 \leqslant E_\alpha \leqslant 10$ MeV [30–32]. We measured the γ-ray angular distribution at three different angles to obtain the remaining two values of $\sigma_{E1}(\gamma_0:E_{\mathrm{c.m.}})$ and $\sigma_{E2}(\gamma_0:E_{\mathrm{c.m.}})/\sigma_{E1}(\gamma_0:E_{\mathrm{c.m.}})$. The $E1$ and $E2$ capture γ-ray yields are sensitive to the yield at $\theta_\gamma = 90^\circ$, 40°, and 130°, respectively. The differential cross section is asymmetrical with respect to $\theta_\gamma = 90^\circ$, depending on the sign of the $E2$ capture amplitude relative to the $E1$ capture amplitude. The attenuation factor, Q_m, resulting from the finite solid angle of each anti-Compton NaI(Tl) spectrometer and the absolute γ-ray detection efficiency was determined, as described later.

The experiment was carried out by changing ^{12}C, ^{197}Au, and ^{27}Al targets cyclically to smear out any possible changes of the measurement system, such as the profile of ^{12}C targets and the resolution of a Si detector. The differential cross section, $d\sigma(E_{\mathrm{c.m.}},\theta)/d\Omega$, was measured relative to the yield

TABLE I. Typical averaged beam intensities and measurement times for ^{12}C, ^{197}Au, and ^{27}Al samples.

E_α (MeV)	I_α (μA)	Measurement time (h)		
		^{12}C	^{197}Au	^{27}Al
2.270	8.1	74	5.5	6.1
2.000	6.2	86	5.6	2.2

of scattered α particles from ^{197}Au$(\alpha,\alpha)^{197}$Au, because its absolute reaction cross section is well known with small uncertainty. All measurement runs were associated with α-beam currents monitored by a Faraday cup. The measurement time, averaged α-beam currents, and integrated charges of He$^+$ ions are listed in Table I.

IV. ANALYSIS AND RESULTS

A. The γ-ray spectrum by bombarding ^{12}C targets with pulsed α-beams

The characteristic γ-ray yield due to ^{12}C$(\alpha,\gamma_0)^{16}$O would be much smaller than background events due to neutrons from ^{13}C$(\alpha,n)^{16}$O, as mentioned before. Hence, we first made a detailed study of the background using a γ-ray spectrum taken at $E_\alpha = 2.000$ MeV, which is useful for the critical study of background events because of the smaller cross section of ^{12}C$(\alpha,\gamma_0)^{16}$O at $E_\alpha = 2.000$ MeV than that at $E_\alpha = 2.270$ MeV. We measured the spectrum by the 40° NaI(Tl) spectrometer, as shown in Fig. 3(a). We clearly see background, such as discrete γ rays at $E_\gamma < 3$ MeV and at $E_\gamma = 6.8$ MeV, and also continuum γ rays up to about 11 MeV, but can hardly see the 8.5-MeV characteristic γ ray from ^{12}C$(\alpha,\gamma_0)^{16}$O because of high background noise.

To determine the origins of the observed discrete and continuum background γ rays, we obtained the TOF spectra by putting the γ-ray energy gate at more 1 MeV and at $7.9 \leqslant E_\gamma \leqslant 8.9$ MeV in Fig. 3(a), as shown in the lower and upper spectra in Fig. 3(b), respectively. Observed events are given as a function of the time relative to the time ($T = 0$ ns) for the events at the ^{12}C target position. In the lower spectrum in Fig. 3(b), we see two peaks at about 15 ns and at about 2 ns, in addition to time-independent constant background events. Note that in the upper spectrum in Fig. 3(b), we see clearly events at $T = 0$ ns, which indicate that there are γ-ray events at $7.9 \leqslant E_\gamma \leqslant 8.9$ MeV, where the characteristic γ-ray from ^{12}C$(\alpha,\gamma_0)^{16}$O should be observed.

Using the obtained TOF spectrum in Fig. 3(b), we identified the origin of these γ rays, as discussed below.

1. Origin of the peak at $T \approx 15$ ns in the TOF spectrum

A typical γ-ray spectrum, which was obtained by putting the TOF gate at $11 \leqslant T \leqslant 17$ ns in the lower spectrum in Fig. 3(b), is shown in Fig. 4(a). Two continuum γ rays up to about 4 and 11 MeV were shown to be due to ^{127}I$(n,n'\gamma)^{127}$I and ^{127}I$(n,\gamma)^{128}$I, respectively, occurring within the 40° central NaI(Tl) detector. First, neutrons with maximum energy of

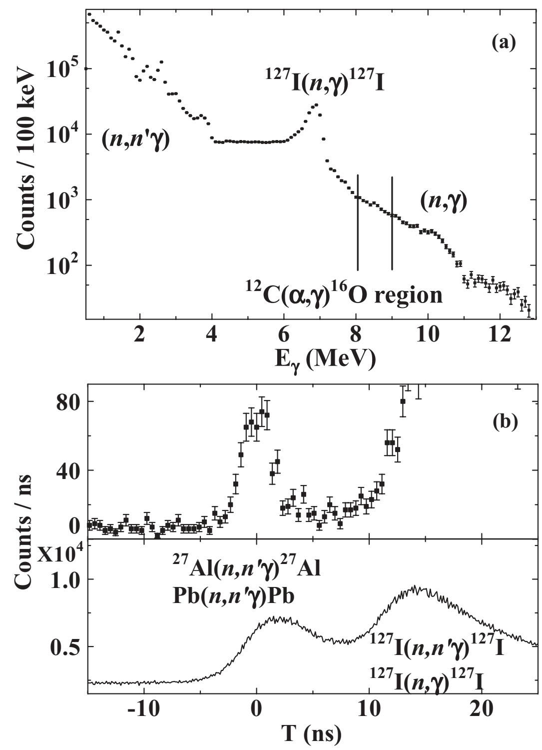

FIG. 3. (a) Typical γ-ray spectrum taken by the 40° NaI(Tl) detector at $E_\alpha = 2.000$ MeV. Here, discrete γ-rays less than 3 MeV were due to $(n,n'\gamma)$ by aluminum and lead. The 6.8-MeV peak was due to the thermal neutron capture by ^{127}I, and the continuum γ rays up to about 4 and 11 MeV were due to $(n,n'\gamma)$ and (n,γ) by ^{127}I and ~4-MeV neutrons, respectively. (b) TOF spectra, which were obtained by putting the γ-ray energy gate above 1 MeV (lower spectrum) and at $7.9 \leqslant E_\gamma \leqslant 8.9$ MeV and 2.000 MeV (upper spectrum). Here, the detected events are shown as a function of the time relative to the time ($T = 0$ ns) for the events at the target position.

~4 MeV were produced by ^{13}C$(\alpha,n)^{16}$O at $E_\alpha = 2.000$ MeV. It took about 15 ns for 4-MeV neutrons to interact with iodine (^{127}I) in the NaI(Tl) detector, which agreed with observed events at the high peak at $T \approx 15$ ns in the TOF spectrum. Here, we took half the length of the central NaI(Tl) detector as an average interaction point between the neutrons and the detector, which was 43.3 cm away from a ^{12}C target. Second, because the maximum neutron energy depends on the emitted angle of neutrons from ^{13}C$(\alpha,n)^{16}$O with respect to the α-beam direction, the observed maximum γ-ray energies resulting from $(n,n'\gamma)$ and (n,γ) by ^{127}I should depend on the angle of the NaI(Tl) spectrometer. Third, because the neutron-separation energy of ^{128}I is 6.83 MeV, γ-ray events up to about 4 and 10.8 MeV could be produced by the $(n,n'\gamma)$ and (n,γ) reactions of ^{127}I with 4-MeV neutrons. Note that because the reactions occur within a NaI(Tl) detector, all cascade γ rays from $(n,n'\gamma)$ and (n,γ) given by ^{127}I to the ground state in ^{128}I could be detected with high efficiency with a large solid angle, making the maximum sum peaks at about 4 and 10.8 MeV. In fact, the observed maximum γ-ray energies in Fig. 4(a) agreed roughly with those (4.01 and 10.84 MeV) calculated by assuming the γ-ray events to be due to the reactions, as given

TABLE II. Maximum energy of neutrons, $E_{n\max}$, from ^{13}C$(\alpha,n)^{16}$O at $E_\alpha = 2.270$ MeV and at $E_\alpha = 2.000$ MeV, entering into the central NaI(Tl) detectors, placed at $\theta_\gamma = 40^\circ, 90^\circ$, and 130°. Observed maximum γ-ray energies from ^{127}I$(n,n'\gamma)^{127}$I, $E_{\gamma\max(n,n'\gamma)}$, and from ^{127}I$(n,\gamma)^{128}$I, $E_{\gamma\max(n,\gamma)}$ agreed roughly with the calculated maximum γ-ray energies.

E_α (MeV)	θ_γ	$E_{n\max}$ (MeV)	$E_{\gamma\max(n,n'\gamma)}$ (MeV)		$E_{\gamma\max(n,\gamma)}$ (MeV)	
			Observed	Calculated	Observed	Calculated
2.270	40°	4.25	∼4.4	4.25	∼11.3	11.08
	90°	3.69	∼4.1	3.69	∼11.1	10.52
	130°	3.28	∼3.9	3.28	∼10.4	10.11
2.000	40°	4.01	∼4.1	4.01	∼11.0	10.84
	90°	3.50	∼4.0	3.50	∼10.9	10.32
	130°	3.12	∼3.5	3.12	∼10.1	9.95

in Table II. As in the case mentioned previously, maximum energies of two continuum γ rays observed by the 40°, 90°, and 130° NaI(Tl) spectrometers at $E_\alpha = 2.270$ MeV and at $E_\alpha = 2.000$ MeV agreed roughly with the calculated ones, as given in Table II.

2. *Origin of the peak at $T \approx 2$ ns in the TOF spectrum*

Similar to the case mentioned previously, the γ-ray spectrum gated by the peak at $T \approx 2$ ns in the lower TOF spectrum in Fig. 3(b) was obtained, as shown in Fig. 4(b). Here, we can see the 1.0-, 1.4-, 1.7-, 2.1-, 2.2-, 2.6-, and 3.0-MeV discrete γ rays and continuum γ rays, which were much suppressed compared to those in Fig. 3(a). The discrete γ rays are considered to be due to $(n,n'\gamma)$ reactions by aluminum and lead with 4-MeV neutrons, as listed in Table III. Note that aluminum and lead were placed at about 5–8 cm away from a ^{12}C target, and it took about 2–3 ns for 4-MeV neutrons to interact with aluminum and lead.

3. *Origin of the constant background in the TOF spectrum*

A γ-ray spectrum was obtained by gating the TOF spectrum in the constant background region of $-44 \leqslant T \leqslant -12$ ns as shown in Fig. 4(c). Note that because we used pulsed α beams with the repetition rate of 4 MHz, we observed constant background during the α-beam-off period, except for the events due to $(n,n'\gamma)$ and (n,γ) reactions, mentioned previously. We can see the 2.2- and 6.8-MeV γ rays from the thermal neutron capture reaction of hydrogen and ^{127}I, respectively, and the 1.5- and 2.6-MeV background γ rays from the β decays of ^{40}K and ^{208}Tl, respectively. Thermal neutrons could be mostly produced by the elastic scattering of 4-MeV neutrons by hydrogen in boron-doped polyethylene with a thickness of 10 cm, placed in front of the 40° central NaI(Tl) detector. The 6.8-MeV γ ray is a characteristic γ ray of thermal-neutron capture by ^{127}I to the ground state of ^{128}I [33]. Although its intensity relative to the total γ-ray intensity is quite weak, less than 0.1%, we see clearly the 6.8-MeV γ-ray peak because all cascade γ rays from ^{127}I$(n,\gamma)^{128}$I to the ground state in ^{128}I occurring within a NaI(Tl) detector could be detected, as discussed previously [34].

Through the previously mentioned studies of background events using a γ-ray spectrum taken at $E_\alpha = 2.000$ MeV, we could understand the origin of main background. Here, it may be worth mentioning that because background events due to $(n,n'\gamma)$ by aluminum and lead were induced by ∼4-MeV neutrons from ^{13}C$(\alpha,n)^{16}$O, they should not affect the characteristic γ-ray events due to ^{12}C$(\alpha,\gamma_0)^{16}$O. However, background events due to (n,γ) by ^{127}I would affect the γ-ray events, because their events were observed up to about 11 MeV, as mentioned previously. Hence, a TOF method should play an important role in the discrimination of the characteristic γ-ray events due to ^{12}C$(\alpha,\gamma_0)^{16}$O from the background events.

In the next subsection, we discuss identification of the characteristic γ ray from ^{12}C$(\alpha,\gamma_0)^{16}$O on the basis of a TOF method, in which we used a γ-ray spectrum taken at $E_\alpha = 2.270$ MeV with high statistics, essential to unambiguously identify the γ-ray peak.

TABLE III. The γ rays, which could be populated by $(n,n'\gamma)$ by ^{27}Al and Pb isotopes, are given.

Nucleus	E_γ (keV)	Placement	Nucleus	E_γ (keV)	Placement
^{27}Al	1014	1014 → 0	^{206}Pb	1344	2148 → 803
	1720	2735 → 1014		1467	1467 → 0
	2212	2212 → 0	^{207}Pb	2092	2662 → 570
	2982	2982 → 0		2132	2702 → 570
	3004	3004 → 0	^{208}Pb	2615	2615 → 0

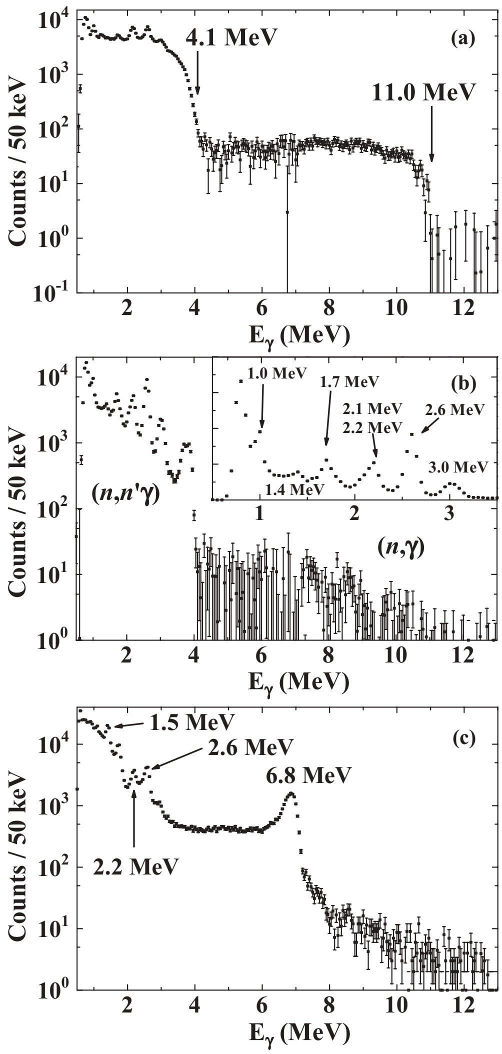

FIG. 4. (a) Typical γ-ray spectrum measured by the 40° NaI(Tl) spectrometer at $E_\alpha = 2.000$ MeV, which was obtained by gating the (lower) TOF spectrum in the region of $11 \leqslant T \leqslant 17$ ns in Fig. 3(b). Continuum γ rays up to about 4.1 MeV and 11 MeV were due to the $(n,n'\gamma)$ and (n,γ) reactions by ^{127}I, respectively. Because constant background was subtracted, the 6.8-MeV peak due to the thermal neutron capture reaction by ^{127}I is not seen. (b) A background-subtracted γ-ray spectrum gated by the peak at $T \approx 2$ ns in the (lower) TOF spectrum. Discrete γ rays from $(n,n'\gamma)$ by aluminum and lead are clearly seen in the inset. Constant background was also subtracted. (c) A γ-ray spectrum gated by the (lower) TOF spectrum in the region of $-44 \leqslant T \leqslant -12$ ns. Here, the 6.8-MeV peak is clearly seen.

B. Identification of the γ ray from ^{12}C$(\alpha,\gamma_0)^{16}$O

1. Response function of NaI(Tl) spectrometer

It should be noted that the γ ray from ^{12}C$(\alpha,\gamma_0)^{16}$O could be clearly identified by accurate determination of observed γ-ray energy and by a detailed comparison of an observed γ-ray spectrum with a calculated one. Therefore, a response function of the NaI(Tl) spectrometer should be determined accurately. In the present study, it was made by convoluting an experimental intrinsic response function of the NaI(Tl) spectrometer, the reaction probability over the ^{12}C target thickness, and the Doppler broadening and shifting of the γ ray, as described here. First, an intrinsic response function of the spectrometer was obtained by adjusting the peak-to-total ratio of a calculated spectrum by the Monte-Carlo code, GEANT4 [35], so as to fit a measured one using the standard γ-ray sources, such as ^{60}Co and ^{88}Y, and γ rays (1.779, 2.383, 5.110, 8.940, and 10.76 MeV) from ^{27}Al$(p,\gamma)^{28}$Si measured at $E_p = 0.992$ and 2.046 MeV. The obtained response function agreed nicely with a measured spectrum [25]. Second, the reaction probability over the ^{12}C target thickness was calculated by taking into account the Coulomb part of the cross section of ^{12}C$(\alpha,\gamma_0)^{16}$O, since the nuclear part of the cross section, an astrophysical S factor, can be assumed to be constant in the present α-beam energy range from 2.270 to 2.000 MeV ($E_{\mathrm{c.m.}} = 1.6$–1.4 MeV), as shown in Fig. 2. Note that three NaI(Tl) spectrometers have their own response functions, depending on an intrinsic response function of the spectrometer, an angle of the spectrometer, θ_γ, the α-beam energy, and a thickness of enriched ^{12}C targets.

2. Indentification of the γ ray from ^{12}C$(\alpha,\gamma_0)^{16}$O

Using a response function and a typical background subtracted (net) spectrum, obtained by the 90° NaI(Tl) spectrometer at $E_\alpha = 2.270$ MeV, the characteristic γ-ray events from ^{12}C$(\alpha,\gamma_0)^{16}$O were identified. A net spectrum was obtained by subtracting a background spectrum from a foreground one (including background) with a TOF method. A TOF spectrum, which was obtained using γ rays from ^{10}B$(\alpha,p\gamma)^{13}$C, was used as a reference TOF spectrum to determine proper TOF gate positions to obtain foreground and background γ-ray spectra. Note that ^{10}B was contained in enriched ^{12}C targets as impurities, and therefore the ^{10}B$(\alpha,p\gamma)^{13}$C reaction occurred at the enriched ^{12}C target position. In addition, we had a sufficient reaction yield of ^{10}B$(\alpha,p\gamma)^{13}$C to determine the gate positions of the TOF spectrum, as discussed later.

A typical TOF spectrum (at $\theta_\gamma = 90°$) obtained by gating the 3.68- and 3.85-MeV γ-ray peaks from ^{10}B$(\alpha,p\gamma)^{13}$C at $E_\alpha = 2.270$ MeV is shown in the lower spectrum in Fig. 5(a) [$E_\alpha = 2.000$ MeV is shown in Fig. 5(b)]. An upper spectrum in Fig. 5(a) [Fig. 5(b)] is a TOF spectrum obtained by gating the γ rays at $8.0 \leqslant E_\gamma \leqslant 9.1$ MeV at $E_\alpha = 2.270$ MeV ($7.9 \leqslant E_\gamma \leqslant 8.9$ MeV at $E_\alpha = 2.000$ MeV) for comparison. Here, to obtain γ-ray events from ^{12}C$(\alpha,\gamma_0)^{16}$O at $E_\alpha =$ 2.270 MeV, TOF gate positions were set at $-6 \leqslant T \leqslant 1.7$ ns [a dashed-dotted line in Fig. 5(a)] for a foreground spectrum and at $-39 \leqslant T \leqslant -7$ ns for a background spectrum, respectively. Note that the TOF gate position on the positive side was set at $T \leqslant 1.7$ ns to get rid of possible events due to (n,γ) by ^{127}I. The obtained foreground and background, and background-subtracted (net), γ-ray spectra are shown in Figs. 6(a) and 6(b), respectively. Note that the net spectrum was obtained by correcting for a finite difference of the TOF gate width between the foreground (width of 7.7 ns) and background (width of 32 ns) spectra. In the foreground spectrum, we can clearly see a γ-ray peak at about 8.7 MeV and several discrete γ-rays at less than ~4.5 MeV.

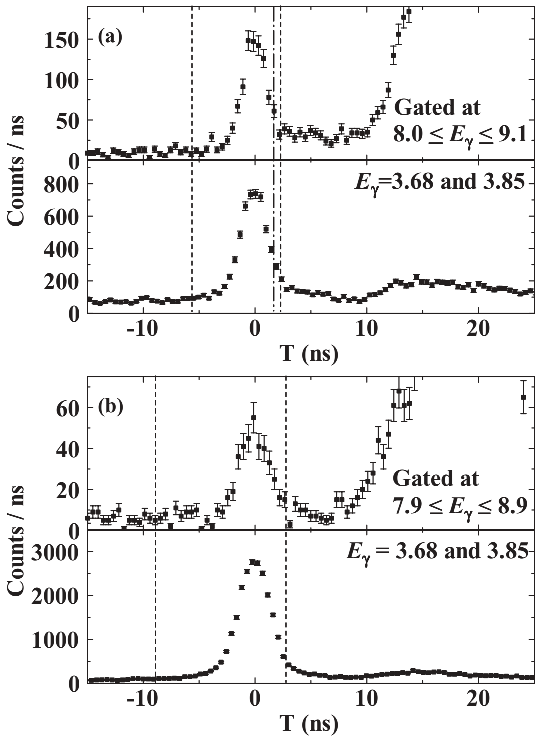

FIG. 5. TOF spectrum taken by the 90° central NaI(Tl) detector at $E_\alpha = 2.270$ MeV (a) and $E_\alpha = 2.000$ MeV (b). Lower and upper spectra in (a) and (b) were obtained by gating 3.68- and 3.85-MeV γ-ray peaks from ^{10}B$(\alpha,p\gamma)^{13}$C and by gating the γ rays at $8.0 \leqslant E_\gamma \leqslant 9.1$ MeV ($7.9 \leqslant E_\gamma \leqslant 8.9$ MeV at $E_\alpha = 2.000$ MeV), respectively. To obtain a net spectrum [Fig. 6(b)], a TOF gate position was set at $-6 \leqslant T \leqslant 1.7$ ns in (a). A dashed-dotted line indicates a gate position at $T = 1.7$ ns. Dotted lines are gate positions, which were used to obtain net yields due to ^{12}C$(\alpha,\gamma_0)^{16}$O, measured by the 90° central NaI(Tl) spectrometer, at $E_\alpha = 2.270$ MeV (a) and $E_\alpha = 2.000$ MeV (b).

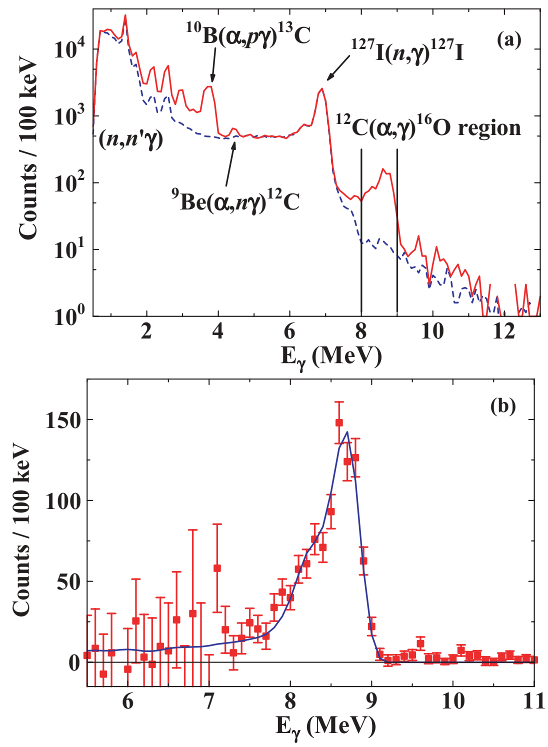

FIG. 6. (Color online) (a) Fore- and background γ-ray spectra taken by the 90° central NaI(Tl) detector at $E_\alpha = 2.270$ MeV. (b) Background-subtracted (net) γ-ray spectrum. The observed 8.7-MeV spectrum fits nicely with the response function of the 90° spectrometer (solid curve).

The observed 8.7-MeV γ-ray peak in Fig. 6(b) was identified as being due to ^{12}C$(\alpha,\gamma_0)^{16}$O. Namely, the energy of the observed 8.7-MeV γ ray was determined accurately to be 8.72 MeV by using the response function of the NaI(Tl) spectrometer and the energy calibration curve of the spectrometer mentioned in Sec. III C. The γ-ray peak energy was in good agreement with the expected energy of the characteristic γ ray from ^{12}C$(\alpha,\gamma_0)^{16}$O by taking into account the Doppler shift and the reaction probability over the ^{12}C target thickness, as given in Table IV. In addition, the observed 8.7-MeV spectrum at $E_\alpha = 2.270$ MeV was fitted well with the response function of the 90° NaI(Tl) spectrometer, as shown in Fig. 6(b). These two facts indicate that the observed 8.7-MeV γ ray was due to the characteristic γ ray of 8.72 MeV from ^{12}C$(\alpha,\gamma_0)^{16}$O.

The 3.68- and 3.85-MeV γ rays in Fig. 6(b) were assigned as due to ^{10}B$(\alpha,p\gamma)^{13}$C and the 4.45-MeV γ ray as due to ^{9}Be$(\alpha,n\gamma)^{12}$C on the basis of the observed energy. Since we saw these γ rays in the foreground spectrum (and also in the net spectrum), both ^{9}Be and ^{10}B were contained in enriched ^{12}C targets as impurities, similar to the cases with old measurements [10,15] using enriched ^{12}C targets with a gold backing and/or enriched ^{12}C targets implanted into a gold foil. In the present study, the quantities of ^{9}Be and ^{10}B were estimated to be about 10^{-7} of ^{12}C using the known cross sections of ^{9}Be$(\alpha,n\gamma)^{12}$C and ^{10}B$(\alpha,p\gamma)^{13}$C at around $E_\alpha = 2.270$ ($E_\alpha = 2.000$) MeV, which are about 60 mb (100 mb) and 120 mb (10 mb) [36], respectively, $\approx 10^7$ times larger than that of ^{12}C$(\alpha,\gamma_0)^{16}$O.

3. TOF gate position and gate width

So far we have discussed the data taken by the 90° NaI(Tl) spectrometer at $E_\alpha = 2.270$ MeV, in which the TOF gate position was temporarily set at $-6 \leqslant T \leqslant 1.7$ ns in the lower

TABLE IV. Observed γ-ray energies from ^{12}C$(\alpha,\gamma_0)^{16}$O, $E_{\gamma\mathrm{obs}}$, measured at $E_\alpha = 2.270$ MeV and $E_\alpha = 2.000$ MeV, are shown to be in agreement with the calculated γ-ray energies, $E_{\gamma\mathrm{cal}}$.

E_α (MeV)	θ_γ	$E_{\gamma\mathrm{obs}}$ (MeV)	$E_{\gamma\mathrm{cal}}$ (MeV)
2.270	40°	8.78	8.816
	90°	8.72	8.733
	130°	8.64	8.670
2.000	40°	8.59	8.616
	90°	8.55	8.541
	130°	8.45	8.482

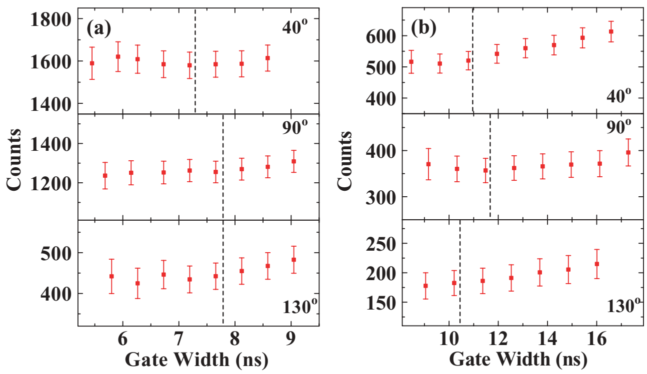

FIG. 7. (Color online) Net yields of the γ ray from $^{12}\mathrm{C}(\alpha,\gamma_0)^{16}\mathrm{O}$ at $\theta_\gamma = 40^\circ, 90^\circ$, and 130° are shown as functions of the gate width on a TOF spectrum at $E_\alpha = 2.270$ MeV (a) and 2.000 MeV (b), respectively. The yields at $\theta_\gamma = 130^\circ$ ($E_\alpha = 2.270$ MeV and $E_\alpha = 2.000$ MeV) and the yield at $\theta_\gamma = 40^\circ$ ($E_\alpha = 2.000$ MeV) increased slightly with increasing the width due to possible events caused by $^{127}\mathrm{I}(n,\gamma)^{128}\mathrm{I}$.

spectrum in Fig. 5(a) to obtain a foreground spectrum. Next, to obtain γ-ray events from $^{12}\mathrm{C}(\alpha,\gamma_0)^{16}\mathrm{O}$ with a good signal-to-noise ratio, we made a detailed study of the gate condition (gate position and gate width) on the TOF spectrum. Here, we set the TOF gate at $-6 \leqslant T \leqslant t_+$ ns (the gate width of $6 + t_+$ ns) for a foreground spectrum and changed the gate width by changing t_+, which is a gate position on the positive side on the TOF spectrum. Note that time-dependent background events resulting from (n,γ) by ^{127}I increased with increasing t_+, as can be seen in Fig. 5(a). We set a gate position on the negative side at the tail of the lower spectrum ($T = -6$ ns), since there were no time-dependent background events at $T < -6$ ns except constant background events, which could be subtracted. A gate position for a background spectrum was set at $-39 \leqslant T \leqslant -7$ ns.

In obtaining a background-subtracted (net) γ-ray yield using a net γ-ray spectrum, which was obtained by subtracting a background γ-ray spectrum from a foreground one, we corrected for a finite difference of the TOF gate width between the foreground and background spectra. In addition, when we compared a net γ-ray yield, which was obtained with a certain gate width, to that obtained with a different gate width, we corrected for a difference between two gate widths. Consequently, a net γ-ray yield was obtained as a function of the gate width on a TOF spectrum, as shown in the middle of Fig. 7(a). The γ-ray yield is almost constant up to the gate width of about 8 ns. Consequently, we determined t_+ to be 2.2 ns in Fig. 5(a), in which a TOF efficiency, mentioned later, was as large as 86%. It should be mentioned that when t_+ is set at $T < 1.5$ ns, for example, accurate determination of the TOF efficiency with an uncertainty of 1.5% would be difficult, since the γ-ray yield in the TOF spectrum changed significantly with changing t_+ at $0 < T < 1.5$ ns.

Here, it should be mentioned that the TOF spectrum obtained in the present measurements depended on each NaI(Tl) spectrometer and α-beam energy. Therefore, we individually set the TOF gate in each measurement. Proper gate conditions were determined for all data obtained by three NaI(Tl) spectrometers at $E_\alpha = 2.270$ and 2.000 MeV, similar to the case mentioned previously. The obtained background-subtracted (net) γ-ray yields at $\theta_\gamma = 40^\circ, 90^\circ$, and 130° are shown at $E_\alpha = 2.270$ and 2.000 MeV in Figs. 7(a) and 7(b), respectively. The net γ-ray yields are almost constant in the regions of the gate width between $\sim$6 and $\sim$8 ns ($\sim$9 and $\sim$11 ns) at $E_\alpha = 2.270$ MeV (at $E_\alpha = 2.000$ MeV). Note that the net yield at $\theta_\gamma = 130^\circ$ at $E_\alpha = 2.270$ MeV, and those at $\theta_\gamma = 40^\circ$ and 130° at $E_\alpha = 2.000$ MeV, increased slightly with increasing gate widths. Events from (n,γ) by ^{127}I could be a possible reason for the increase, since the events up to about 11 MeV were observed, as discussed previously.

By referring to the results in Figs. 7(a) and 7(b) and also by considering TOF efficiency, which is discussed later, we determined the TOF gate width of each NaI(Tl) spectrometer at a point, shown as a dotted line in Figs. 7(a) and 7(b), slightly narrower than a full width of a TOF spectrum [see Figs. 5(a) and 5(b)].

4. Background-subtracted (net) γ-ray spectra from $^{12}\mathrm{C}(\alpha,\gamma_0)^{16}\mathrm{O}$

On the basis of the gate widths determined previously, background-subtracted (net) γ-ray spectra were obtained, as shown in Figs. 8(a)–8(f). As in the case mentioned previously, the peak energy of an observed γ ray in these figures was shown to be in good agreement with the expected energy of the characteristic γ ray from $^{12}\mathrm{C}(\alpha,\gamma_0)^{16}\mathrm{O}$, as given in Table IV. The observed spectra with high statistics also fitted well with response functions of the NaI(Tl) spectrometers. These two facts clearly indicate that the observed γ rays were due to the characteristic γ ray from $^{12}\mathrm{C}(\alpha,\gamma_0)^{16}\mathrm{O}$.

5. Origin of the 7.5-MeV γ-ray peak

In Fig. 8, we see a weak γ-ray peak at 7.5 MeV at $E_\alpha = 2.000$ MeV. Although we could obtain the γ-ray yield from $^{12}\mathrm{C}(\alpha,\gamma_0)^{16}\mathrm{O}$ almost free from the 7.5-MeV γ-ray event, we tried to understand the origin of the 7.5-MeV γ-ray event by measuring a γ-ray spectrum by bombarding three samples of a natural C target (with a gold backing, gold foil, and aluminum foil) with an α-beam. Note that since we see the 7.5-MeV γ ray in Figs. 8(d)–8(f), a possible origin of the γ ray was considered to be an impurity in the enriched ^{12}C sample. Gold foil and aluminum were used as a backing for enriched ^{12}C targets and a target chamber, respectively. Note that the natural C target was made by the same method as for enriched ^{12}C targets.

The γ-ray spectrum for a natural C sample is shown in Fig. 9, in which we can clearly see the 7.5-MeV peak with a smaller yield of the 8.55-MeV one from $^{12}\mathrm{C}(\alpha,\gamma_0)^{16}\mathrm{O}$. We did not observe the peak for gold and aluminum samples. Hence, the 7.5-MeV γ-ray event was considered to originate from an α-induced reaction on impurities contained in ^{12}C targets. Identification of the reaction channel for producing the 7.5-MeV γ-ray event remains an open problem.

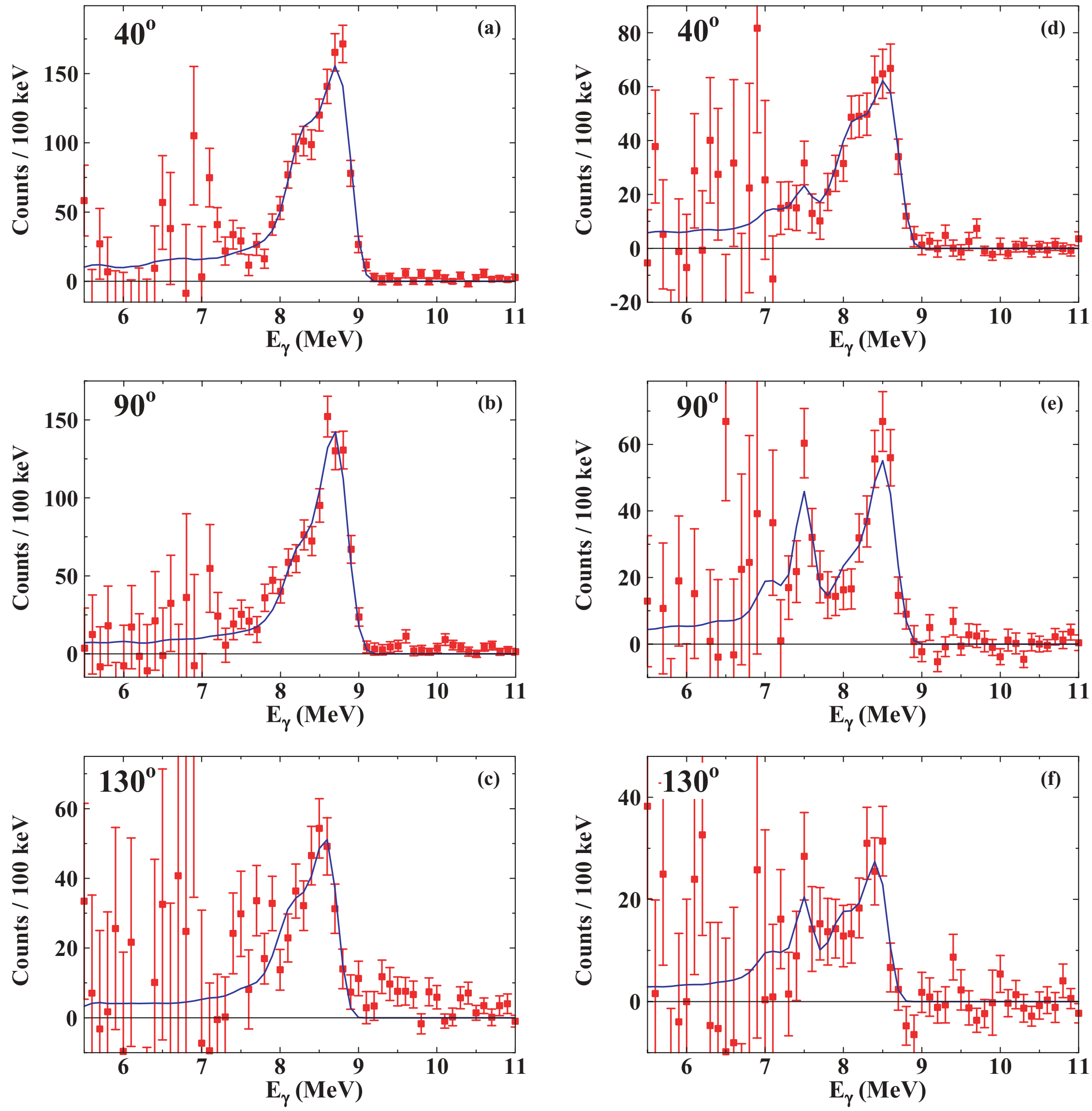

FIG. 8. (Color online) Background-subtracted (net) γ-ray spectra in the energy range from 5.5 to 11 MeV obtained by the 40° (a) [(d)], 90° (b) [(e)], and 130° (c) [(f)] NaI(Tl) spectrometers, at $E_\alpha = 2.270$ MeV ($E_\alpha = 2.270$ MeV). Here, solid lines are the calculated spectra using the response function of the NaI(Tl) spectrometers by taking account of the Doppler shift of the γ ray from $^{12}\mathrm{C}(\alpha,\gamma_0)^{16}\mathrm{O}$ and the thickness of ^{12}C targets.

C. The γ-ray yield from $^{12}\mathrm{C}(\alpha,\gamma_0)^{16}\mathrm{O}$

1. Observed γ-ray yield and γ-ray detection efficiency of anti-Compton NaI(Tl) spectrometer

The γ-ray yield, $Y_\gamma(E_{\mathrm{c.m.}})$, of $^{12}\mathrm{C}(\alpha,\gamma_0)^{16}\mathrm{O}$ was obtained by integrating the yield of the γ-ray peak region, as given in Table V. The region of integration was determined by referring to a fitted curve of the mentioned response function of the NaI(Tl) spectrometer to the observed γ-ray peak including the single escape peak in the measured net spectrum to minimize the χ^2 of the difference between the calculated yields and the observed peak yields. The absolute γ-ray detection efficiency of each anti-Compton NaI(Tl) spectrometer, $\epsilon_\gamma(E_\gamma)$, was measured using the standard γ-ray sources and γ rays from $^{27}\mathrm{Al}(p,\gamma)^{28}\mathrm{Si}$ mentioned previously by integrating observed counts over an observed γ-ray peak region, including the single escape peak. Since the energy dependence of the measured $\epsilon_\gamma(E_\gamma)$ agreed with the one calculated by GEANT4 with an uncertainty of 3% [25], we extrapolated the measured efficiency curve using the calculated energy dependence of efficiency. The obtained $\epsilon_\gamma(E_\gamma)$ for the γ ray from $^{12}\mathrm{C}(\alpha,\gamma_0)^{16}\mathrm{O}$ is given in Table V.

2. Attenuation factor of the NaI(Tl) spectrometer

The NaI(Tl) spectrometer had a finite solid angle against enriched ^{12}C samples, and therefore a measured γ-ray angular distribution from a nuclear reaction showed a

TABLE V. Thickness of enriched ^{12}C target, integrated α particles (ϕ_α), angle of the NaI(Tl) spectrometer (θ_γ), γ-ray yield from the ^{12}C(α,γ_0)^{16}O reaction to the ground state of ^{16}O (Y_γ), γ-ray detection efficiency of the NaI(Tl) spectrometer (ϵ_γ), and TOF correction factor (ϵ_{TOF}).

E_α (MeV)	Target thickness (μg/cm^2)	ϕ_α ($\times 10^{19}$)	θ_γ	Y_γ	ϵ_γ ($\times 10^{-3}$)	ϵ_{TOF}
2.270			40°	1203(42)	7.14	0.837(19)
	374(4)	1.061	90°	983(36)	7.01	0.864(19)
			130°	380(29)	6.43	0.834(20)
2.000			40°	502(27)	7.14	0.929(14)
	294(4)	1.038	90°	361(25)	7.20	0.928(15)
			130°	196(21)	6.55	0.917(15)

smeared distribution. An attenuation factor of the spectrometer due to the solid angle was calculated for the cylindrical 228.6-mm-diam by 203.2-mm-long NaI(Tl) detector with uniform efficiency across its surface using a formula given in Ref. [37]. The results are listed in Table VI. It was shown that the measured angular distribution of γ ray from the ^{27}Al(p,γ)^{28}Si reaction at $E_p = 2.046$ MeV was nicely reproduced using the obtained attenuation factors [25], which validated the obtained attenuation factors. Note that the angular-distribution measurement was performed by using an aluminum target with a thickness of 30 μg/cm^2 at four angles of 0°, 40°, 90°, and 130° with respect to the proton beam direction. The calculated coefficients were used in an analysis of the γ-ray angular distribution of the ^{12}C(α,γ_0)^{16}O reaction.

3. *TOF correction ϵ_{TOF}*

We put a gate width on a TOF spectrum narrower than its full width to obtain a net γ-ray spectrum from ^{12}C(α,γ_0)^{16}O with a good signal-to-noise ratio, as mentioned before. Consequently, the ratio of the obtained net yield to that obtained with the full width, ϵ_{TOF}, is smaller than 1, and the value $1/\epsilon_{\mathrm{TOF}}$ gives a correction factor for the thus-determined TOF width. The ϵ_{TOF} was derived accurately by using the TOF spectrum with high statistics, which was obtained using the 3.68- and 3.85-MeV γ rays from ^{10}B($\alpha,p\gamma$)^{13}C occurring at the enriched ^{12}C target position, as shown in Fig. 5. The obtained ϵ_{TOF} values are listed in Table V.

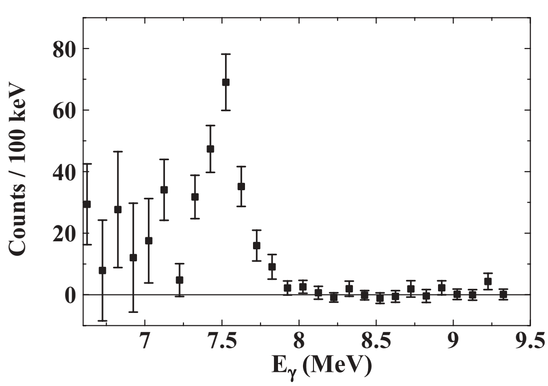

FIG. 9. A γ-ray spectrum obtained by bombarding a natural carbon target with α beam of $E_\alpha = 2.000$ MeV. We see clearly the 7.5-MeV γ-ray peak.

Through the studies of the characteristic γ ray from ^{12}C(α,γ_0)^{16}O, we could obtain the observed γ-ray yields of all NaI(Tl) spectrometers, measured at $E_\alpha = 2.270$ MeV and $E_\alpha = 2.000$ MeV, by using their γ-ray efficiencies and the TOF correction factors. In the next subsection, we discuss the thickness of enriched ^{12}C targets and a number of incident α particles obtained by using a RBS.

D. RBS spectrum

1. *RBS spectrum*

A typical RBS spectrum of ^{12}C targets irradiated for a certain amount of integrated beam currents at $E_\alpha = 2.270$ MeV is shown in Fig. 10(a). Events at the high-energy edge at around 2.1 MeV and the low-energy edge at around 1.0 MeV were due to the scattering of α particles from gold and ^{12}C, respectively. All enriched ^{12}C targets used in the present study changed their depth profile gradually with increasingly integrated α-beam currents. We replaced a ^{12}C target with a new one when we found the RBS spectrum lost its steepness at the low-energy edge at around 1 MeV.

2. *Number of incident α particles ϕ_α and ^{12}C target thickness*

The absolute number of incident α particles, ϕ_α, and a thickness of enriched ^{12}C targets were determined, as given in Table V for measurements at $E_\alpha = 2.270$ MeV and $E_\alpha = 2.000$ MeV, by analyzing the measured RBS spectrum of α particles scattered by a ^{12}C target with a gold backing with the use of the computer program SIMNRA [38]. In the program, energy straggling due to electronic- and nuclear-energy

TABLE VI. An attenuation factor of the NaI(Tl) spectrometer [25].

θ_γ	Q_1	Q_2	Q_3	Q_4
40°	0.980	0.947	0.898	0.837
90°	0.980	0.946	0.897	0.835
130°	0.980	0.948	0.901	0.841

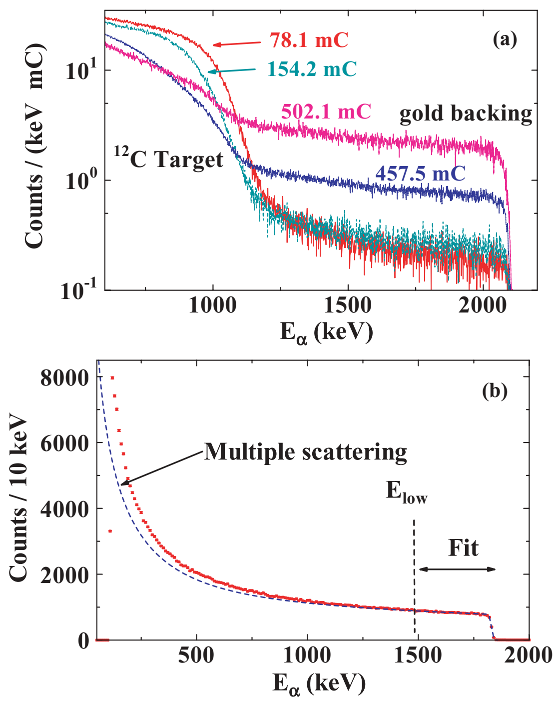

FIG. 10. (Color online) (a) Depth profile of an enriched ^{12}C target. The label for each spectrum indicates integrated charges of α particle on the ^{12}C target. (b) Comparison of the measured RBS spectrum (solid line) at $E_\alpha = 2.000$ MeV with the calculated one (dotted line) using Rutherford cross sections.

losses as well as energy resolution of a detector were taken into account in calculating the depth profile of a ^{12}C target.

A typical measured RBS spectrum is compared to a calculated one by SIMNRA in Fig. 10(b). Here, it should be mentioned that since a low-energy part of the measured RBS spectrum is known to deviate from the one calculated by SIMNRA, mostly because of the multiple scattering of incident α particles in a sample, it was necessary to determine the lowest energy, E_{low}, that could be used to fit a calculated spectrum to a measured RBS spectrum. Note that multiple scattering effects become important at lower energy and for a thick sample. The energy E_{low} was determined by minimizing the χ^2:

$$\chi^2 = \frac{1}{N_\alpha} \sum_{E=E_{\text{low}}}^{E_{\text{max}}} \left\{ \frac{Y_\alpha^{\text{exp}}(E_k) - \epsilon_{\text{FC}} Y_\alpha^{\text{calc}}(E_k)}{\delta Y_\alpha^{\text{exp}}(E_k)}^2 \right\}, \quad (2)$$

where E_{max} is the maximum energy of an α particle scattered by a sample, $Y_\alpha^{\text{exp}}(E_k)$ was the measured yield of α particles with energy E_k, $Y_\alpha^{\text{calc}}(E_k)$ was the calculated value, and $\delta Y_\alpha^{\text{exp}}(E_k)$ is an experimental error of $Y_\alpha^{\text{exp}}(E_k)$, respectively. The parameter N_α is the number of data points in the RBS spectrum. The parameter ϵ_{FC} is the normalization factor of α-beam currents measured by a Faraday cup to monitor an instantaneous change of α-beam currents. It was determined so that the measured total α-beam current would be equal to the calculated α-beam intensity. Note that a certain fraction of secondary electrons, which were produced by bombarding a Faraday cup with an α beam, would leave the Faraday cup, because the depth of the Faraday cup was shallow, about 2 cm, and the opening was 2.2 cm in diameter, despite that a suppressor ring was placed in front of the target to suppress secondary electrons by applying a negative voltage of 350 V. The thus-obtained ϵ_{FC} was 0.928 ± 0.013.

The quoted uncertainty of the thicknesses of enriched ^{12}C targets is a result of combined uncertainties of the statistics of the yield, energy calibration of a silicon detector, and the calculation of the energy loss of the incident α particle in enriched ^{12}C targets. Here, it should be mentioned that because we used enriched ^{12}C targets with a gold backing instead of ^{12}C targets implanted into a gold plating to reduce any systematic uncertainties due to the ^{12}C homogeneity in the implanted ^{12}C targets and the α-beam position, we could accurately determine a target thickness within an uncertainty of 1% and the effective reaction energy. Note that when the energy is determined with an uncertainty of 40 keV at $E_{\text{eff}} \approx 1.4$ MeV, $\sigma_{E1}(\gamma_0 : E_{\text{eff}})$ would have an uncertainty of $\sim$20% because of the high sensitivity of $\sigma_{E1}(\gamma_0 : E_{\text{eff}})$ to E_{eff}.

V. DISCUSSION

A. Differential cross section of the ^{12}C$(\alpha,\gamma_0)^{16}$O reaction and effective energy

The differential cross section of ^{12}C$(\alpha,\gamma_0)^{16}$O was derived. We used enriched ^{12}C targets with a thickness of about 300 μg/cm^2. Incident α beams would lose their energy by about 400 keV in the targets. Since the differential cross section, $d\sigma(E_{\text{c.m.}},\theta_\gamma)/d\Omega$, of ^{12}C$(\alpha,\gamma_0)^{16}$O drops steeply with decreasing α-beam energy in a target, the reaction yield, $Y(E_{\text{c.m.}},\theta_\gamma)$, observed at an angle θ_γ, is given as an integration of $d\sigma(E_{\text{c.m.}},\theta_\gamma)/d\Omega$ over the target thickness ΔE_t (in units of keV):

$$Y(E_{\text{c.m.}},\theta) = \epsilon_\gamma \phi_\alpha \epsilon_{\text{TOF}} \int_{E_\alpha - \Delta E_t}^{E_\alpha} \left\{ \frac{[d\sigma(E_{\text{c.m.}},\theta)/d\Omega]}{\epsilon(E_{\text{c.m.}})} \right\} dE. \quad (3)$$

Here, ϵ_γ, ϕ_α, and ϵ_{TOF} are the γ-ray detection efficiency of an anti-Compton NaI(Tl) spectrometer, the number of incident α particles, and the correction factor for the loss of the γ-ray yield due to the TOF cut mentioned previously, respectively. The parameter, $\epsilon(E_{\text{c.m.}})$, is the stopping cross section of the α beam in the ^{12}C targets:

$$\epsilon(E_{\text{c.m.}}) = \left(\frac{1}{n}\right)\left(\frac{dE}{dx}\right), \quad (4)$$

where dx is the target thickness, dE/dx is the energy-loss rate of the α beam, and n is the number of target nuclei per unit volume. The value ΔE_t was calculated by using a measured RBS spectrum and a computer program, SRIM [39], to be about 517 keV (436 keV) for the ^{12}C target with a thickness of 374 μg/cm^2 (294 μg/cm^2) for α beams of $E_\alpha = 2.270$ MeV (2.000 MeV). Because of the change of the ^{12}C$(\alpha,\gamma_0)^{16}$O reaction cross section in the targets, we defined the effective α-beam energy, E_{eff}, associated with an observed reaction yield so that the γ-ray yield in the energy range from $E_{\text{c.m.}}$ to

TABLE VII. Results of the present experiment: differential cross section, $d\sigma(E_{\rm eff},\theta_\gamma)/d\Omega$ at $\theta_\gamma = 40^\circ$, 90°, and 130°; effective reaction energy ($E_{\rm eff}$); relative phase ($\cos\Phi$) between the $E1$ and $E2$ capture components of the ^{12}C(α,γ_0)^{16}O reaction; the $E1$ and $[\sigma_{E1}(\gamma_0 : E_{\rm eff})]$ and $E2$ $[\sigma_{E2}(\gamma_0 : E_{\rm eff})]$ capture cross sections; and astrophysical $E1$ $[S_{E1}(\gamma_0 : E_{\rm eff})]$, and $E2$ $[S_{E2}(\gamma_0 : E_{\rm eff})]$ S factors. The experimental uncertainties, given in brackets, were calculated by taking a quadratic sum of statistical and systematic errors of the present experiment.

E_α (MeV)	θ_γ	$\frac{d\sigma(E_{\rm c.m.},\theta)}{d\Omega}$ (pb/sr)	$E_{\rm eff}$ (MeV)	$\cos\Phi$	σ_{E1} (nb)	σ_{E2}/σ_{E1}	σ_{E2} (nb)	S_{E1} (keV b)	S_{E2} (keV b)
2.270	40°	106.0(66)							
	90°	85.8(55)	1.591	0.626	0.735(48)	0.289(62)	0.212(48)	14.1(9)	4.07(91)
	130°	37.4(39)							
2.000	40°	51.0(38)							
	90°	36.4(33)	1.407	0.592	0.308(32)	0.426(115)	0.131(38)	14.7(15)	6.25(181)
	130°	22.0(28)							

$E_{\rm eff}$ would be equal to half of the γ-ray yield for the full target thickness [40]:

$$\int_{E_\alpha-\Delta E_t}^{E_\alpha}\left\{\frac{[d\sigma(E_{\rm c.m.},\theta)/d\Omega]}{\epsilon(E_{\rm c.m.})}\right\}dE = 2\int_{E_{\rm eff}}^{E_\alpha}\left\{\frac{[d\sigma(E_{\rm c.m.},\theta)/d\Omega]}{\epsilon(E_{\rm c.m.})}\right\}dE. \tag{5}$$

In Eqs. (3) and (5), we assumed that the differential cross section decreases with decreasing the α-beam energy, in accordance with the Coulomb force between an α particle and a carbon. This assumption is reasonable in the present α-beam energy range between 2.227 and 2.000 MeV. The thus-determined effective energies, $E_{\rm eff}$, were 1.591 ± 0.003 and 1.407 ± 0.003 MeV for incident α beams of 2.270 and 2.000 MeV, respectively. The quoted uncertainty of the effective energy is the result of the combined uncertainties of the accelerating voltage, the energy calibration of a silicon detector, and of the calculation of the energy loss of the incident α particle in the targets. Using $Y(E_{\rm eff},\theta_\gamma)$, ϵ_γ, ϕ_α, and $\epsilon_{\rm TOF}$, we determined the $d\sigma(E_{\rm eff},\theta_\gamma)/d\Omega$ at $\theta_\gamma = 40^\circ$, 90°, and 130° for $E_\alpha = 2.270$ and 2.000 MeV, as given in Table VII. We could nicely fit the thus-obtained $d\sigma(E_{\rm eff},\theta_\gamma)/d\Omega$ at $E_\alpha = 2.270$ and 2.000 MeV by using Eq. (1) with fixed phase angles $\Phi(E)$ of 51.2° and 53.7°as shown in Figs. 11(a) and 11(b), respectively. Here, $\Phi(E)$ was obtained from a recent ^{12}C(α,α)^{12}C scattering experiment [32]. The thus-determined $\sigma_{E1}(\gamma_0 : E_{\rm eff})$ and $\sigma_{E2}(\gamma_0 : E_{\rm eff})$ values are listed in Table VII. Note that since $\Phi(E)$ was determined accurately with a small uncertainty of 1.5°, its uncertainty does not affect the obtained $\sigma_{E1}(\gamma_0 : E_{\rm eff})$ and $\sigma_{E2}(\gamma_0 : E_{\rm eff})$ within their uncertainties. Here, the quoted uncertainty is the result of combined uncertainties of statistical and systematic errors, such as the γ-ray yield statistics, the γ-ray detection efficiency (3%) of the NaI(Tl) spectrometer, and the solid angle of a silicon detector (3%), respectively. The uncertainties related to a correction factor for the Faraday cup, $\epsilon_{\rm FC}$, due to secondary electrons (1.4%), the gain shift of a silicon detector (1%), the estimation of energy loss in the carbon target (1%), and effective reaction energy (2%) were small.

B. Comparison of the present $\sigma_{E1}(\gamma_0 : E_{\rm eff})$ and $\sigma_{E2}(\gamma_0 : E_{\rm eff})$ to old data

The present results of $\sigma_{E1}(\gamma_0 : E_{\rm eff})$ were compared to the previous ones, which were obtained by an absolute measurement of $\sigma_{E1}(\gamma_0 : E_{\rm c.m.})$ at $1.0 < E_{\rm c.m.} < 1.7$ MeV, as shown in Fig. 12. Uncertainties in the present data were estimated by taking a quadratic sum of the statistical and systematic errors. [Note that some results of the previous $\sigma_{E1}(\gamma_0 : E_{\rm c.m.})$ were obtained by normalizing the measured γ-ray yield from ^{12}C(α,γ_0)^{16}O at $E_{\rm c.m.} \approx 2.36$ MeV to the averaged value of $\sigma(E_{\rm c.m.} = 2.36$ MeV), as mentioned before,

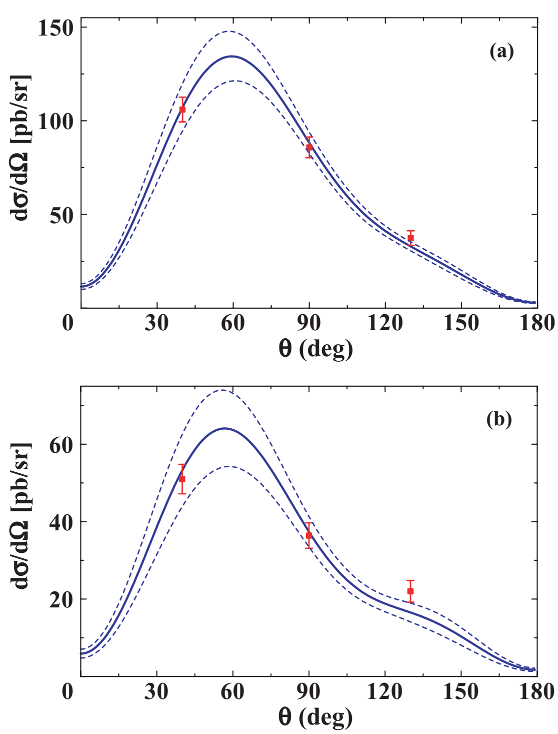

FIG. 11. (Color online) The γ-ray angular distributions of ^{12}C(α,γ_0)^{16}O at $E_\alpha = 2.270$ MeV (a) and $E_\alpha = 2.000$ MeV (b), respectively. The best fit of the angular distributions (solid line) using Eq. (1) with the fixed-phase Φ is shown together with angular distributions (dotted line) obtained by taking into account experimental errors of $\sigma_{E1}(\gamma_0 : E_{\rm eff})$ and $[\sigma_{E2}(\gamma_0 : E_{\rm eff})]/[\sigma_{E1}(\gamma_0 : E_{\rm eff})]$ in Eq. (1).

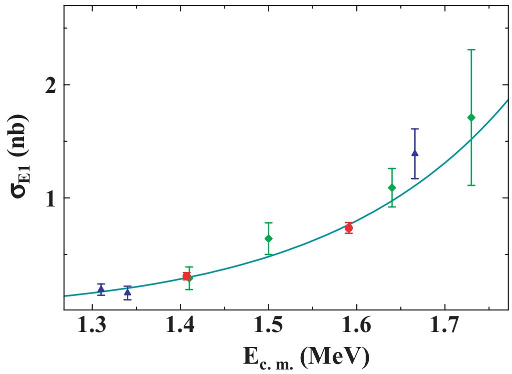

FIG. 12. (Color online) Present results of $\sigma_{E1}(\gamma_0 : E_{\rm eff})$ (filled circle) are compared to the previous ones, which were obtained by an absolute measurement of $\sigma_{E1}(\gamma_0 : E_{\rm c.m.})$ at $1.0 \leqslant E_{\rm c.m.} \leqslant 1.7$ MeV (filled diamond [3], filled triangle [20], and solid line [21]). The uncertainty of the present data was estimated by taking a quadratic sum of the statistical and systematic errors.

and they are not shown in Fig. 12.] In the present study, we succeeded in accurately determining $\sigma_{E1}(\gamma_0 : E_{\rm eff})$ at $E_{\rm eff} = 1.591$ and 1.407 MeV, and results agree with previous ones [3,20] within the experimental uncertainties. It should be stressed that the present $\sigma_{E1}(\gamma_0 : E_{\rm eff})$ values are in excellent agreement with the values, $\sigma_{E1}(E_{\rm c.m.})_{R-{\rm matrix}}$, derived by a fitted curve (solid line) on the basis of the R-matrix calculation [21]. In fact, the uncertainty of $\sigma_{E1}(E_{\rm c.m.})_{R-{\rm matrix}}$ was determined experimentally for the first time by the present accurate measurement of $\sigma_{E1}(\gamma_0 : E_{\rm eff})$ to be less than 6% and 9% at $E_{\rm eff} = 1.591$ and 1.407 MeV, respectively. Note that $\sigma_{E1}(E_{\rm c.m.})_{R-{\rm matrix}}$ was obtained using previous $\sigma_{E1}(E_{\rm c.m.})$ [3,10,14,41], as described before.

The total cross section, $\sigma(\gamma_0 : E_{\rm eff})$, which was obtained by adding the present $\sigma_{E1}(\gamma_0 : E_{\rm eff})$ and $\sigma_{E2}(\gamma_0 : E_{\rm eff})$, was compared to the previous one [13], as shown in Fig. 13. The present data are much smaller than the previous data.

In regards to the $E2$ cross section, $\sigma_{E2}(\gamma_0 : E_{\rm eff})$, we could determine $\sigma_{E2}(\gamma_0 : E_{\rm eff})$ better than that of previous works [10,15–17,20], as shown in Figs. 14(a)–14(f). The present $\sigma_{E2}(\gamma_0 : E_{\rm eff})$ mostly agrees with those in Refs. [10,15,17,20]

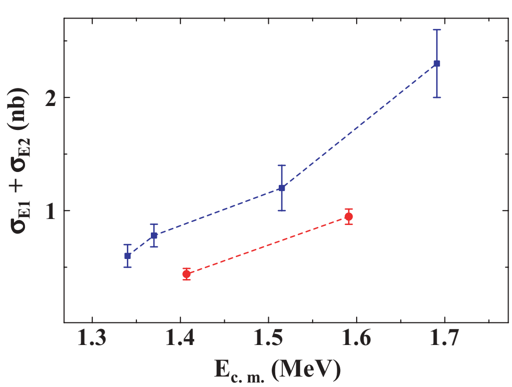

FIG. 13. (Color online) Sum of the present $\sigma_{E1}(\gamma_0 : E_{\rm eff})$ and $\sigma_{E2}(\gamma_0 : E_{\rm eff})$ (filled circle) is compared to the previous one, which was obtained by an absolute measurement of $\sigma(\gamma_0 : E_{\rm c.m.})$ at $1.0 \leqslant E_{\rm c.m.} \leqslant 1.7$ MeV (filled rectangle [13]).

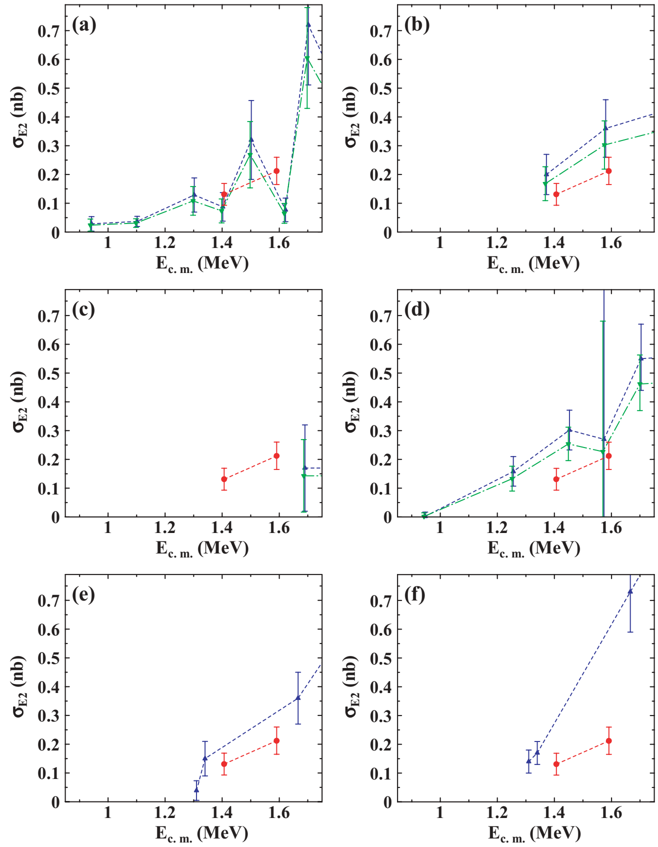

FIG. 14. (Color online) Present $\sigma_{E2}(\gamma_0 : E_{\rm eff})$ (filled circle) is compared to the previous data one by one: (a) [10], (b) [15], (c) [16], (d) [17], (e) (fixed phase: two parameters) [20], and (f) (free phase: three parameters) [20].

within their experimental uncertainties, although the present values are smaller than the central values of the previous data. Note that previous data of $\sigma_{E2}(\gamma_0 : E_{\rm c.m.})$ were mostly derived by ratio measurements of $\sigma_{E2}(\gamma_0 : E_{\rm eff})$ to $\sigma_{E1}(\gamma_0 : E_{\rm eff})$, except for the latest measurement [20]. Here it should be mentioned again that the present results of $\sigma_{E1}(\gamma_0 : E_{\rm eff})$ were found to agree with the previous measurement [3], and the $\sigma_{E1}(\gamma_0 : E_{\rm c.m.} = 2.32$ MeV) of 39.53 ± 1.31 nb [3] is smaller than an averaged value $\sigma(\gamma_0 : E_{\rm c.m.} = 2.36$ MeV) of 47 ± 3 nb by about 20%. Hence, when one uses $\sigma_{E1}(\gamma_0 : E_{\rm c.m.})$ of 39.53 ± 1.31 nb to derive $\sigma_{E2}(\gamma_0 : E_{\rm c.m.})$ by using the ratio measurements, the agreement of the present $\sigma_{E2}(\gamma_0 : E_{\rm eff})$ with those of previous data becomes better, as shown in Figs. 14(a), 14(b), and 14(d). However, the latest measurement [20] was obtained by an absolute measurement of $\sigma_{E2}(\gamma_0 : E_{\rm eff})$, in which the γ-ray angular-distribution data were analyzed using the phase angle, Φ, in Eq. (1) to be fixed and/or to be a free parameter. Note that the value $\sigma_{E2}(\gamma_0 : E_{\rm eff})$ obtained by the former method shown in Fig. 14(e) differed from the latter one at the lowest energy $E_{\rm eff} = 1.314$ MeV shown in Fig. 14(f). The value is larger than that by the latter one at $E_{\rm eff} \leqslant 2.267$ MeV, and the thus-determined phase shifts by the latter analysis were different from those obtained by elastic α-scattering measurements. The reason for the discrepancy remains an open

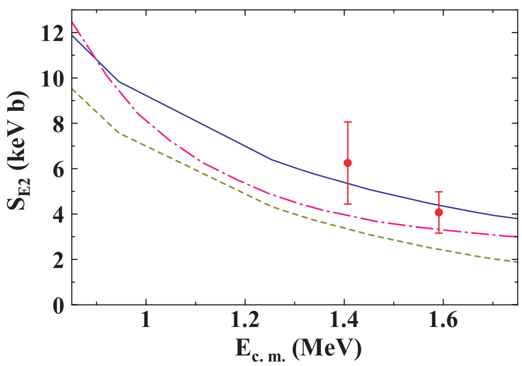

FIG. 15. (Color online) Comparison of the present astrophysical $E2$ S factor $S_{E2}(\gamma_0 : E_{\rm eff})$ (full circle) with theoretical ones with two different phase coefficients (see text): solid line (set A in Ref. [7]), dotted line (set B in Ref. [7]), and dashed-dotted line [5].

question [20]. The latest data [20] were analyzed in the same way as we analyzed our data when a γ-ray peak was clearly observed. Namely, the peak energy and the line shape of an observed γ-ray peak were confirmed to meet the conditions that characterized the γ ray from ^{12}C$(\alpha,\gamma_0)^{16}$O. We stress that it is of vital importance to clearly observe a γ-ray peak from ^{12}C$(\alpha,\gamma_0)^{16}$O with a good signal-to-noise ratio and to check the characteristic features of the peak to reliably determine the γ-ray yield.

C. Comparison of the present astrophysical $S_{E2}(\gamma_0 : E_{\rm eff})$ factor to calculated ones

We derived astrophysical $S_{E1}(\gamma_0 : E_{\rm eff})$ and $S_{E2}(\gamma_0 : E_{\rm eff})$ factors from the obtained $\sigma_{E1}(\gamma_0 : E_{\rm eff})$ and $\sigma_{E2}(\gamma_0 : E_{\rm eff})$, as given in Table VII, and the thus-obtained $S_{E2}(\gamma_0 : E_{\rm eff})$ was compared to theoretical values [5,7], as shown in Fig. 15. In Ref. [5], the $S_{E2}(\gamma_0 : E_{\rm c.m.})$ factor was derived by simultaneously fitting it to the experimental data [10] and the ^{12}C + α d-wave phase shift [31]. In Ref. [7], the $S_{E2}(\gamma_0 : E_{\rm c.m.})$ factor was obtained by using the subthreshold 2^+ asymptotic normalization constant provided by the generator-coordinate method in the R-matrix fit. Here, the capture cross section of ^{12}C$(\alpha,\gamma_0)^{16}$O was calculated by using the phase coefficients, ϵ_1, ϵ_2, ϵ_3, and ϵ_4, to indicate the sign of the electromagnetic matrix elements for the 2^+ states at the subthreshold $E = -0.245$ MeV, the resonances at $E = 2.68$ and 4.36 MeV, and a background term at 10 MeV, respectively. The derived $S_{E2}(\gamma_0 : E_{\rm c.m.})$ factor depends on the combinations of three phase coefficients, ϵ_2, ϵ_3, and ϵ_4, assuming $\epsilon_1 = +1$. The present $S_{E2}(\gamma_0 : E_{\rm eff})$ is in good agreement with the calculated one [7] (solid line), in which one of the interference signs can be rejected. Dufour and Descouvemont recommended a $S_{E2}(\gamma_0 : 300$ keV) of 42 ± 2 keV b [7], and Azuma *et al.* recommended a $S_{E1}(\gamma_0 : 300$ keV) of 79 ± 21 keV b [21], which in turn gives a total $S(\gamma_0 : 300$ keV) factor of 121 ± 21 keV b.

VI. CONCLUSION

We measured the γ-ray angular distribution from ^{12}C$(\alpha,\gamma_0)^{16}$O to the ground state of ^{16}O using a newly constructed measurement system. An intense pulsed α beam together with a high-efficiency anti-Compton NaI(Tl) spectrometer played a crucial role in detecting the γ ray with a good signal-to-noise ratio, free from neutron-induced background events, with a TOF method. The thus-obtained γ-ray spectrum showed unique features characterizing the γ ray from ^{12}C$(\alpha,\gamma_0)^{16}$O, such as the line shape of the Doppler broadened peak and the energy loss of α particles in the ^{12}C targets. An RBS spectrum of α particles from enriched ^{12}C targets taken online gave precise information on the target thickness during beam irradiation and incident α-beam intensities with little uncertainty. Consequently, we could accurately determine the absolute $E1$ and $E2$ cross sections for the γ-ray transition with small statistical and systematic uncertainties at $E_{\rm eff} =$ 1.6 and 1.4 MeV. The present $S_{E1}(\gamma_0 : E_{\rm eff})$ and $S_{E2}(\gamma_0 : E_{\rm eff})$ factors agree nicely with the values derived by the R-matrix calculation of the β-delayed α spectrum of ^{16}N and by using the asymptotic normalization constant in the R-matrix fit. On the basis of the good agreement, we report $S(\gamma_0 : 300$ keV) to be 121 ± 21 keV b. Finally, the method employed in the present study turned out to be very powerful and reliably determined $\sigma_{E1}(\gamma_0 : E_{\rm c.m.})$ and $\sigma_{E2}(\gamma_0 : E_{\rm c.m.})$ with small systematic and statistical uncertainties at a low α-beam energy.

ACKNOWLEDGMENTS

We thank I. Sugai, Y. Takeda, T. Kajino, S. Okabe, N. Iwamoto, and P. Descouvemont for useful discussions and K. Tosaka for his reliable operation of the Pelletron accelerator. This work was supported by a Grant-in-Aid for Scientific Research from the Japan Ministry of Education, Culture, Sports, Science, and Technology.

[1] T. A. Weaver and S. E. Woosley, Phys. Rep. **227**, 65 (1993).
[2] M. Hashimoto, Prog. Theor. Phys. **94**, 663 (1995).
[3] P. Dyer and C. A. Barnes, Nucl. Phys. **A233**, 495 (1974).
[4] J. Humblet, B. W. Filippone, and S. E. Koonin, Phys. Rev. C **48**, 2114 (1993).
[5] F. C. Barker and T. Kajino, Aust. J. Phys. **44**, 369 (1991).
[6] C. Angulo and P. Descouvemont, Phys. Rev. C **61**, 064611 (2000).
[7] M. Dufour and P. Descouvemont, Phys. Rev. C **78**, 015808 (2008).
[8] L. Buchmann, R. E. Azuma, C. A. Barnes, J. Humblet, and K. Langanke, Phys. Rev. C **54**, 393 (1996).
[9] D. R. Tilley, H. R. Weller, and C. M. Cheves, Nucl. Phys. **A564**, 1 (1993).
[10] A. Redder, H. W. Becker, C. Rolfs, H. P. Trautvetter, T. R. Donoghue, T. C. Rinckel, J. W. Hammer, and K. Langanke, Nucl. Phys. **A462**, 385 (1987).
[11] C. Matei *et al.*, Phys. Rev. Lett. **97**, 242503(4) (2006).
[12] S. Harissopulos, H. W. Becker, J. W. Hammer, A. Lagoyannis, C. Rolfs, and F. Strieder, Phys. Rev. C **72**, 062801(R) (2005).

[13] K. U. Kettner, H. W. Becker, L. Buchmann, J. Görres, H. Kräwinkel, C. Rolfs, P. Schmalbrock, H. P. Trautvetter, and A. Vlieks, Z. Phys. A **308**, 73 (1982).
[14] R. M. Kremer, C. A. Barnes, K. H. Chang, H. C. Evans, B. W. Filippone, K. H. Hahn, and L. W. Mitchell, Phys. Rev. Lett. **60**, 1475 (1988).
[15] J. M. L. Ouellet *et al.*, Phys. Rev. C **54**, 1982 (1996).
[16] G. Roters, C. Rolfs, F. Strieder, and H. Trautvetter, Eur. Phys. J. A **6**, 451 (1999).
[17] R. Kunz, M. Jaeger, A. Mayer, J. W. Hammer, G. Staudt, S. Harissopulos, and T. Paradellis, Phys. Rev. Lett. **86**, 3244 (2001).
[18] L. Gialanella *et al.*, Eur. Phys. J. A **11**, 357 (2001).
[19] D. Schürmann *et al.*, Eur. Phys. J. A **26**, 301 (2005).
[20] M. Assunção *et al.*, Phys. Rev. C **73**, 055801 (2006).
[21] R. E. Azuma *et al.*, Phys. Rev. C **50**, 1194 (1994).
[22] X. D. Tang *et al.*, Phys. Rev. Lett. **99**, 052502 (2007).
[23] C. R. Brune, W. H. Geist, R. W. Kavanagh, and K. D. Veal, Phys. Rev. Lett. **83**, 4025 (1999).
[24] A. Belhout *et al.*, Nucl. Phys. **A793**, 178 (2007).
[25] H. Makii, K. Mishima, M. Segawa, E. Sano, H. Ueda, T. Shima, Y. Nagai, M. Igashira, and T. Ohsaki, Nucl. Instrum. Methods Phys. Res. A **547**, 411 (2005).
[26] I. Sugai, Y. Takeda, H. Kawakami, Y. Nagai, and N. Ohta, Nucl. Instrum. Methods Phys. Res. A **590**, 164 (2008).
[27] K. Shibata *et al.*, J. Nucl. Sci. Technol. **39**, 1125 (2002).
[28] T. Ohsaki, Y. Nagai, M. Igashira, T. Shima, T. S. Suzuki, T. Kikuchi, T. Kobayashi, T. Takaoka, M. Kinoshita, and Y. Nobuhara, Nucl. Instrum. Methods Phys. Res. A **425**, 302 (1999).
[29] F. C. Barker, Aust. J. Phys. **40**, 25 (1987).
[30] M. D'Agostino Bruno, I. Massa, A. Uguzzoni, G. Vannini, E. Verondini, and A. Vitale, Nuovo Cimento A **27**, 1 (1975).
[31] R. Plaga, H. W. Becker, A. Redder, C. Rolfs, H. P. Trautvetter, and K. Langanke, Nucl. Phys. **A465**, 291 (1987).
[32] P. Tischhauser *et al.*, Phys. Rev. Lett. **88**, 072501 (2002).
[33] M. Chadwick *et al.*, Nucl. Data Sheets **107**, 2931 (2006).
[34] Y. Nagai, T. Kikuchi, T. Kii, T. S. Suzuki, T. Murakami, T. Shima, and T. Ohsaki, Nucl. Instrum. Methods Phys. Res. A **368**, 498 (1996).
[35] S. Agostinelli *et al.*, Nucl. Instrum. Methods Phys. Res. A **506**, 250 (2003).
[36] T. W. Bonner, A. A. Kraus, J. B. Marion, and J. P. Schiffer, Phys. Rev. **102**, 1348 (1956).
[37] M. E. Rose, Phys. Rev. **91**, 610 (1953).
[38] M. Mayer, Max-Planck Institut für Plasmaphysik Technical Report, 2006 (unpublished).
[39] J. F. Ziegler, *The Stopping and Ranges of Ions in Materials*, SRIM program version 97.06 (1997).
[40] C. Rolfs and W. S. Rodney, *Caudrons in the Cosmos* (University of Chicago Press, Chicago, 1988).
[41] J. M. L. Ouellet *et al.*, Phys. Rev. Lett. **69**, 1896 (1992).